

Complete Nagy-Soper subtraction for next-to-leading order calculations in QCD

G. Bevilacqua, M. Czakon, M. Kubocz and M. Worek

Institut für Theoretische Teilchenphysik und Kosmologie, RWTH Aachen University, D-52056 Aachen, Germany

E-mail: bevilacqua@physik.rwth-aachen.de,
mczakon@physik.rwth-aachen.de, kubocz@physik.rwth-aachen.de,
worek@physik.rwth-aachen.de

ABSTRACT: We extend the HELAC-DIPOLES package with the implementation of a new subtraction formalism, first introduced by Nagy and Soper in the formulation of an improved parton shower. We discuss a systematic, semi-numerical approach for the evaluation of the integrated subtraction terms for both massless and massive partons, which provides the missing ingredient for a complete implementation. In consequence, the new scheme can now be used as part of a complete NLO QCD calculation for processes with arbitrary parton masses and multiplicities. We assess its overall performance through a detailed comparison with results based on Catani-Seymour subtraction. The importance of random polarization and color sampling of the external partons is also examined.

KEYWORDS: NLO Computations, Standard Model, QCD Phenomenology, Hadronic Colliders, Monte Carlo Simulations

TTK-13-20

Contents

| | | |
|----------|--|-----------|
| 1 | Introduction | 1 |
| 2 | General framework of subtraction at NLO QCD | 2 |
| 3 | The Nagy-Soper formalism | 6 |
| 3.1 | Notation | 6 |
| 3.2 | Momentum mapping | 7 |
| 3.3 | Splitting functions | 9 |
| 3.4 | Phase space factorization | 13 |
| 4 | Integration over the unresolved phase space | 14 |
| 4.1 | Splitting variables | 14 |
| 4.2 | Semi-numerical approach | 17 |
| 5 | Implementation in HELAC-DIPOLES | 21 |
| 6 | Numerical Study | 24 |
| 6.1 | Input parameters and phase space cuts | 24 |
| 6.2 | Comparisons with the Catani-Seymour scheme | 25 |
| 6.3 | Random color and polarization sampling | 28 |
| 7 | Conclusions and Outlook | 30 |
| A | Configuration of HELAC-DIPOLES | 31 |

1 Introduction

Recent years have seen a tremendous progress in next-to-leading order (NLO) calculations [1–27]. Most it was due to the development of new methods [28–36] and the perfecting of traditional approaches [37–40] to the calculation of virtual corrections. In practical applications, however, most computational time is spent on the evaluation of real radiation corrections. The latter are not considered a technical obstacle, because of subtraction schemes, which allow to reduce the problem to the application of ordinary Monte Carlo methods and were already introduced in the 90’s [41, 42]. This paper is concerned with another subtraction scheme, named after Z. Nagy and D. Soper, and based on a new concept of a parton shower presented in [43–45]. The ideas of the latter publication have already been partly exploited in a series of papers [46–48]. The present publication is meant to complete the construction for all cases of practical interest.

Since the Nagy-Soper subtraction scheme is based on a parton shower, it should be obvious that our main motivation is to provide a framework for simple matching between a fixed order calculation and the new parton shower. This topic will be tackled in future publications. Here, we wish to solve the problem of the integration of subtraction terms over the unresolved phase space. This is the non-trivial part of any subtraction scheme. Contrary to the usual practice at NLO, we will not perform involved analytic integrations. After a suitable parameterization, we will perform the integrations numerically much in the spirit of most recent NNLO methods [49]. This will allow us to cover both massless and massive cases with similar effort. At the same time, we will argue that the cost of the numerical integrations in applications may be neglected. This semi-numerical approach is what sets us apart from the publications [46–48].

In order to exploit the available tools as much as possible, we will integrate the new subtraction scheme within the HELAC-DIPOLES framework [50], which already provides most of the ingredients, *i.e.* the color and spin correlated tree-level matrix elements and the Monte Carlo integration system. We will also demonstrate the capabilities of our system on a few challenging examples.

This paper is organized as follows: in the next section, section 2, we will review the concept of subtraction schemes and point out the differences between the most used Catani-Seymour subtraction [42, 51] and the Nagy-Soper subtraction; subsequently, we will present the details of the Nagy-Soper approach, *i.e.* momentum mappings, splitting and soft functions and phase space factorizations; in section 4, we will explain our approach to the integration of subtraction terms, while in section 5 we will discuss the implementation inside HELAC-DIPOLES; section 6 will contain numerical comparisons between our implementation of the Nagy-Soper and Catani-Seymour subtractions, together with an assessment of overall performance of random polarization and color sampling.

2 General framework of subtraction at NLO QCD

Let us consider a generic process involving $m + 1$ external QCD partons with momenta $p_a + p_b \rightarrow p_1 + \dots + p_{m-1}$: we outline the method for the most general case where an unresolved parton can be radiated off either the initial or the final state, typical of a hadron collider. The same approach applies to other cases as well, such as e^+e^- colliders, with some conceptual simplifications that will be clear in the following. The inclusive cross section, at NLO QCD accuracy, reads

$$\sigma_{\text{NLO}} = \int_m d\Phi_m \mathcal{A}^B(\{p\}_m) F_m \quad (2.1)$$

$$+ \int_{m+1} d\Phi_{m+1} \mathcal{A}^R(\{p\}_{m+1}) F_{m+1} \quad (2.2)$$

$$+ \int_m d\Phi_m \mathcal{A}^V(\{p\}_m) F_m \quad (2.3)$$

$$+ \int_0^1 dx \int_m d\Phi_m(x) \mathcal{A}^C(x, \{p\}_m) F_m \quad (2.4)$$

where we have neglected (in the remainder of this section as well) the global flux, statistical, spin and color averaging factors, moreover

$$\mathcal{A}^B \equiv |\mathcal{M}^{\text{Born}}|^2, \quad \mathcal{A}^R \equiv |\mathcal{M}^{\text{Real}}|^2, \quad \mathcal{A}^V \equiv 2 \Re [\mathcal{M}^{\text{Born}} (\mathcal{M}^{\text{1-Loop}})^*], \quad (2.5)$$

where $\mathcal{M}^{\text{Born}}$, $\mathcal{M}^{\text{1-Loop}}$, $\mathcal{M}^{\text{Real}}$ represent the Born, one-loop and real-emission matrix elements respectively. We denote with $d\Phi_m$ the integration measure for a m -parton phase space and with F_m the jet function which shapes the kinematically accessible regions of it.

When the kinematics of the final state is characterized by m well separated hard jets, the Born contribution is finite, whereas the virtual and the real-emission terms are individually divergent due to the presence of singularities of various nature: ultraviolet for \mathcal{A}^V , and soft/collinear for both \mathcal{A}^V and \mathcal{A}^R . As it is well known, when using an infrared-safe definition of partonic jets, all soft and collinear divergencies that affect the virtual and real corrections cancel in the sum, with one notable exception: the singularities arising from the emission of nearly-collinear partons off the initial state. In fact, the latter are reabsorbed into a re-definition of the parton distribution functions (PDFs) that is achieved by introducing suitable *collinear counterterms*, \mathcal{A}^C . In the $\overline{\text{MS}}$ scheme with $d = 4 - 2\epsilon$ dimensions, these counterterms read as follows,

$$\int_0^1 dx \int_m d\Phi_m(x) \mathcal{A}^C(x, \{p\}_m) F_m = \quad (2.6)$$

$$= \frac{\alpha_s}{2\pi} \frac{1}{\Gamma(1-\epsilon)} \sum_k \int_0^1 dx \int_m d\Phi_m(x) \mathcal{A}_{ak}^B(xp_a, p_b) \frac{1}{\epsilon} \left(\frac{4\pi\mu_R^2}{\mu_F^2} \right)^\epsilon P_{ak}(x) F_m \quad (2.7)$$

$$+ \frac{\alpha_s}{2\pi} \frac{1}{\Gamma(1-\epsilon)} \sum_k \int_0^1 dx \int_m d\Phi_m(x) \mathcal{A}_{bk}^B(p_a, xp_b) \frac{1}{\epsilon} \left(\frac{4\pi\mu_R^2}{\mu_F^2} \right)^\epsilon P_{bk}(x) F_m. \quad (2.8)$$

Here $P_{ab}(x)$ are the Altarelli-Parisi kernels in four dimensions [52], while μ_R , μ_F denote the renormalization and factorization scale respectively. We use the symbolic notation " $d\Phi_m(x)$ " to underline that the kinematically available phase space depends upon the value of the integration variable x , since the square of the center-of-mass energy of the partonic system (neglecting parton masses) is $\hat{s}(x) = 2xp_a \cdot p_b$. Also, it should be clear that in all cases where no initial-state QCD radiation is possible, as for example in the case of e^+e^- collisions, no contribution from the collinear counterterms is necessary.

As a consequence of the cancellations, and after ultraviolet renormalization is performed, the inclusive cross section σ_{NLO} is a finite quantity. However, the individual pieces still suffer from soft and collinear divergencies and cannot be integrated numerically in four dimensions. A possible way to overcome this issue is to regularize the integrands by adding and subtracting local counterterms, \mathcal{A}^D , designed to match the singular structure in the

soft and collinear limits:

$$\sigma_{\text{NLO}} = \int_m d\Phi_m \mathcal{A}^B(\{p\}_m) F_m \quad (2.9)$$

$$+ \int_{m+1} d\Phi_{m+1} [\mathcal{A}^R(\{p\}_{m+1}) F_{m+1} - \mathcal{A}^D(\{p\}_{m+1}) F_m] \quad (2.10)$$

$$+ \int_0^1 dx \int_m d\Phi_m(x) \left[\delta(1-x) \left(\mathcal{A}^V(\{p\}_m) + \int_1 \mathcal{A}^D(\{p\}_{m+1}) \right) \right. \\ \left. + \mathcal{A}^C(x, \{p\}_m) \right] F_m. \quad (2.11)$$

As in the case of the real-emission terms, the local counterterms \mathcal{A}^D are defined on the $(m+1)$ -parton phase space, denoted $\{p\}_{m+1}$. They are subtracted from \mathcal{A}^R and added back to \mathcal{A}^V after integration over the phase space of the unresolved parton. The outlined *subtraction method* makes the integrals (2.10) and (2.11) individually convergent and thus well suited for a Monte Carlo integration.

The construction of the local counterterms is inspired by the well known property of the universal factorization of QCD amplitudes in the soft and collinear limits. Schematically, the singular structure of a $(m+1)$ -parton squared amplitude for two partons p_i and p_j becoming collinear can be approximated as follows:

$$\langle \mathcal{M}(\{p\}_{m+1}) | \mathcal{M}(\{p\}_{m+1}) \rangle_{\text{sing}} \approx \langle \mathcal{M}(\{\bar{p}\}_m^{(ij)}) | (\mathbf{V}_{ij}^\dagger \cdot \mathbf{V}_{ij}) | \mathcal{M}(\{\bar{p}\}_m^{(ij)}) \rangle.$$

Here $|\mathcal{M}(\{\bar{p}\}_m)\rangle$ is an amplitude describing m on-shell external partons and \mathbf{V} is an operator acting on the spin part of the amplitude, while $\{\bar{p}\}_m^{(ij)}$ represents the m -parton kinematics to which $\{p\}_{m+1}$ reduces in the limit where partons p_i and p_j are strictly collinear: the two splitting partons merge to form a new on-shell parton, $\bar{p}_i \equiv p_i \pm p_j$ (the sign depends whether the splitting occurs in the final or in the initial state), while the remaining momenta are left unchanged. In other words, using our standard notation, in the regions of the phase space where the pair (p_i, p_j) is nearly collinear, the structure of the real-emission contribution simplifies to

$$\mathcal{A}^R(\{p\}_{m+1}) \approx \mathcal{A}^B(\{\bar{p}\}_m^{(ij)}) \otimes \mathcal{C}^{(ij)}(\bar{p}_i; p_i, p_j). \quad (2.12)$$

Namely, it reduces to the product of a finite Born squared amplitude times a divergent, collinear splitting kernel \mathcal{C}^{ij} associated with the splitting $\bar{p}_i \rightarrow p_i + p_j$. The symbol \otimes denotes here spin correlations. On the other hand, when a parton p_j becomes soft, factorization takes the form

$$\langle \mathcal{M}(\{p\}_{m+1}) | \mathcal{M}(\{p\}_{m+1}) \rangle_{\text{sing}} \approx \sum_{k \neq j} \langle \mathcal{M}(\{\bar{p}\}_m^{(j)}) | (\mathbf{T}_i \cdot \mathbf{T}_k) | \mathcal{M}(\{\bar{p}\}_m^{(j)}) \rangle,$$

where \mathbf{T} is an operator acting on the color part of the amplitude and $\{\bar{p}\}_m^{(j)}$ is the soft limit of the kinematical configuration $\{p\}_{m+1}$, where $\bar{p}_i \equiv p_i$ and the remaining momenta are left unchanged. Using our notation, in the nearly-soft limit where $p_j \rightarrow 0$, one can write

$$\mathcal{A}^R(\{p\}_{m+1}) \approx \sum_{k \neq j} \mathcal{A}^B(\{\bar{p}\}_m^{(j)}) \otimes \mathcal{S}^{(kj)}(\bar{p}_i, \bar{p}_k; p_i, p_k, p_j), \quad (2.13)$$

and the factorization is expressed in terms of m soft splitting kernels $\mathcal{S}^{(kj)}$, one for each external parton. The symbol \otimes denotes here color correlations.

The outlined factorization properties suggest a general rule for constructing the local counterterms within the subtraction method. First, one needs to define a complete set of transformations which map the original phase space $\{p\}_{m+1}$ into a new space of m on-shell partons, called $\{\tilde{p}\}_m$:

$$\{p\}_{m+1} \rightarrow \{\tilde{p}\}_m^{(\ell)} \quad , \quad \ell = \{1, \dots, N\} . \quad (2.14)$$

By complete, we mean that for each pair (p_i, p_j) becoming collinear, there is at least one mapping $\{\tilde{p}\}_m^{(\ell)}$ that smoothly approaches the singular kinematical configuration $\{\bar{p}\}_m^{(ij)}$. Similarly, for each parton p_j becoming soft, there is at least one ℓ such that $\{\tilde{p}\}_m^{(\ell)} \rightarrow \{\bar{p}\}_m^{(j)}$.

Second, one needs to define a set of splitting functions $\mathcal{D}^{(\ell)}(\{\tilde{p}\}_m, \{p\}_{m+1})$, that match the behavior of the soft and collinear kernels in the singular limits. Then, the local counterterms take the general form:

$$\mathcal{A}^D(\{p\}_{m+1}) = \sum_{\ell=1}^N \mathcal{A}^B(\{\tilde{p}\}_m^{(\ell)}) \otimes \mathcal{D}^{(\ell)}(\{\tilde{p}\}_m^{(\ell)}, \{p\}_{m+1}) . \quad (2.15)$$

There is of course a certain freedom in defining both mappings and splitting functions away from the singular limits, each choice leading to a different subtraction scheme. Perhaps the most widespread version is the Catani-Seymour (CS) scheme [42, 51], where one has

$$\mathcal{A}_{\text{CS}}^D(\{p\}_{m+1}) = \sum_{i,j,k=1}^{m+1} \mathcal{A}^B(\{\tilde{p}\}_m^{(ijk)}) \otimes \mathcal{D}_{\text{CS}}^{(ijk)}(\{\tilde{p}\}_m^{(ijk)}, \{p\}_{m+1}) . \quad (2.16)$$

In this scheme, each mapping $\{\tilde{p}\}_m^{(ijk)}$ is labeled by three parton indexes. We note that for large numbers m of external partons, the number of mappings and matrix elements required by the calculation scales cubically: $N_{\text{CS}} \sim m^3$. For comparison, in the Nagy-Soper (NS) scheme one has

$$\mathcal{A}_{\text{NS}}^D(\{p\}_{m+1}) = \sum_{i,j,k=1}^{m+1} \mathcal{A}^B(\{\tilde{p}\}_m^{(ij)}) \otimes \mathcal{D}_{\text{NS}}^{(ijk)}(\{\tilde{p}\}_m^{(ij)}, \{p\}_{m+1}) \quad (2.17)$$

$$= \sum_{i,j} \mathcal{A}^B(\{\tilde{p}\}_m^{(ij)}) \otimes \left(\sum_k \mathcal{D}_{\text{NS}}^{(ijk)}(\{\tilde{p}\}_m^{(ij)}, \{p\}_{m+1}) \right) , \quad (2.18)$$

namely each mapping is characterized by two labels $\{ij\}$ only, which implies that $N_{\text{NS}} \sim m^2$. Thus, the number of mappings and subsequent matrix element re-evaluations is reduced asymptotically by a factor m compared to CS, which makes the NS scheme most appealing for processes with large jet multiplicities. As will be clear in Section 3, the reduced number of subtraction terms is achieved at the price of a more complicated $\{\tilde{p}\}_m$ kinematics. This, in turn, makes the integration over the phase space of the unresolved parton more challenging. This sort of complementarity of features provides a strong motivation for a comparative analysis of the two subtraction methods, that is one goal of the present paper.

In the Nagy-Soper scheme, the overall structure of the calculation for the genuine real-emission contribution to σ_{NLO} takes the following form:

$$\sigma_{\text{RE}} \equiv \int_{m+1} d\Phi_{m+1} [\mathcal{A}^R(\{p\}_{m+1}) F_{m+1} - \sum_{i,k,j=1}^{m+1} \mathcal{A}^B(\{\tilde{p}\}_m^{(ij)}) \otimes \mathcal{D}^{(ijk)}(\{\tilde{p}\}_m^{(ij)}, \{p\}_{m+1}) F_m] \quad (2.19)$$

$$+ \sum_{i,k=1}^m \int_m d\Phi_m \mathcal{A}^B(\{p\}_m) \otimes \mathbf{I}^{(ik)}(\epsilon, \{p\}_m) F_m \quad (2.20)$$

$$+ \sum_{i=\{a,b\}} \sum_{k=1}^m \int_0^1 dx \int_m d\Phi_m(x) \mathcal{A}^B(x, \{p\}_m) \otimes [\mathbf{K}^{(ik)}(x, \{p\}_m) + \mathbf{P}^{(ik)}(x, \mu_F^2)] F_m. \quad (2.21)$$

There are three kinds of contributions: the first one, (2.19) is the *subtracted real* part, while the remaining two represent the *integrated subtraction terms*. Using standard notation, (2.20) is the universal $\mathbf{I}(\epsilon)$ operator, which encodes the full soft/collinear structure of the matrix element in the form of single and double ϵ poles, together with a finite part. The third one, Eq.(2.21), is the \mathbf{KP} operator, which consists of purely finite pieces coming from the initial-state splitting (\mathbf{K}) as well as from the collinear counterterms (\mathbf{P}). It involves an additional integration over the momentum fraction x of an incoming parton after splitting. The overall sum σ_{RE} of the three contributions is independent on the subtraction scheme employed.

3 The Nagy-Soper formalism

3.1 Notation

First of all, it is necessary to set up a notation for the description of the parton kinematics and splitting. Let us consider a generic reaction involving $m+1$ external partons, where we label particles and the corresponding momenta by an index which takes values $l \in \{a, b\}$ for the initial state, and $l \in \{1, \dots, m-1\}$ for the final state. Let Q be the total momentum:

$$Q = p_a + p_b = \sum_{l=1}^{m-1} p_l. \quad (3.1)$$

In the Nagy-Soper formalism, each subtraction term highlights two partonic momenta p_i and p_j out of the $m+1$ available, in such a way that it reproduces the divergent structure of the amplitude when the two momenta reach the soft/collinear limits. These two momenta uniquely characterize the mapping $\{\tilde{p}\}_m^{(ij)}$ and thus the subtraction term itself. We will refer to p_i, p_j as to the *splitting momenta* while the remaining partons, also called *spectators*, will be labeled with $\{k_1, \dots, k_{m-1}\}$. As to the splitting momenta, we will always assume

$p_j^2 = 0$, whereas p_i may have an arbitrary mass $p_i^2 = m_i^2$ ¹. Furthermore, we introduce the following quantities

$$P_{ij} \equiv p_i + p_j \quad \text{for } i \in \{1, \dots, m-1\} \quad (3.2)$$

$$P_{ij} \equiv p_i - p_j \quad \text{for } i \in \{a, b\}. \quad (3.3)$$

$$K \equiv Q - P_{ij} \quad \text{for } i \in \{1, \dots, m-1\} \quad (3.4)$$

$$K \equiv Q - p_j \quad \text{for } i \in \{a, b\}. \quad (3.5)$$

A divergence occurs when $P_{ij}^2 \rightarrow m_i^2$, that is when p_j is arbitrarily soft and/or, in case $m_i^2 = 0$, when it is arbitrarily collinear to p_i . K is the so-called *collective spectator* and coincides with the sum of all spectator momenta.

3.2 Momentum mapping

The momentum mapping $\{p\}_{m+1} \rightarrow \{\tilde{p}\}_m^{(ij)}$ relates momenta before and after the splitting in the following way:

$$P_{ij} \rightarrow \tilde{p}_i, \quad (3.6)$$

$$k_l \rightarrow \tilde{k}_l, \quad l \in \{1, \dots, m-1\}. \quad (3.7)$$

Two basic constraints must be satisfied. First, all partons must be on-shell according to the rules

$$\tilde{p}_i^2 = p_i^2, \quad (3.8)$$

$$\tilde{k}_l^2 = k_l^2, \quad l \in \{1, \dots, m-1\}. \quad (3.9)$$

For clarity, we remark that the relation $\tilde{p}_i^2 = p_i^2$ is true for all QCD splittings with the exception of $g \rightarrow Q\bar{Q}$, where Q is a massive quark. As already mentioned, at this stage we do not associate any subtraction term to this kind of (non-singular) splittings. For this reason we can take (3.8) as a general rule in the context of this paper.

As a second constraint, the mapping must reduce to a simple identity in the singular limits, namely

$$P_{ij}^2 = m_i^2 \quad \Rightarrow \quad \tilde{p}_i = P_{ij}, \quad \tilde{k}_i = k_i. \quad (3.10)$$

It should be clear that the identity $\tilde{p}_i = P_{ij}$ is no longer compatible with the onshellness condition (3.8) away from the singular limits, hence \tilde{p}_i requires in general an additional contribution in order to remain on-shell. The extra momentum components are taken from

¹We point out that, in general, also the splitting parton p_j can have a mass, $p_j^2 = m_j^2$. In QCD, this is the case of the splitting $g \rightarrow Q\bar{Q}$, where Q is a massive quark. Note however that in this case, also known as *quasi-collinear* splitting, the quark mass regulates the collinear divergence, while there is no soft singularity. The quasi-collinear splitting functions are thus fully regular, although enhanced by logarithms of m_j^2 which could limit the convergence of the numerical integration in case of very small values of m_j . With the goal of improving stability, one may implement additional local subtraction terms to cope with such regular splittings as well, as done for example in [51]. We leave this implementation for future developments.

the spectator partons in a way that is not unique, depending whether the splitting occurs in the initial or in the final state.

We begin our exposition considering the case where the splitting parton belongs to the final state. Following Ref. [43], the momentum of the splitting parton is defined to lie on the Q - P_{ij} plane according to the formula

$$P_{ij} = \beta \tilde{p}_i + \gamma Q, \quad (3.11)$$

where the parameters β and γ are uniquely fixed by setting

$$\tilde{Q} = Q, \quad (3.12)$$

$$\tilde{K}^2 = K^2 \quad (3.13)$$

together with the constraint $\tilde{p}_i^2 = m_i^2$. We remind that all kinematical quantities marked with the symbol "tilde" belong to the mapped m -parton phase space. In other words, the Nagy-Soper mapping acts in such a way that the total momentum Q and the invariant mass K^2 of the collective spectator are left unchanged. This gives

$$\beta = 2 \sqrt{\frac{(P_{ij} \cdot Q)^2 - P_{ij}^2 Q^2}{(m_i^2 + 2 P_{ij} \cdot Q - P_{ij}^2)^2 - 4 m_i^2 Q^2}}, \quad (3.14)$$

$$\gamma = \frac{2 P_{ij} \cdot Q + \beta (P_{ij}^2 - 2 P_{ij} \cdot Q - m_i^2)}{2 Q^2}. \quad (3.15)$$

In the singular limit one gets $P_{ij}^2 = m_i^2$, $\beta = 1$ and $\gamma = 0$, thus $\tilde{p}_i = P_{ij}$ as required. As to the spectator partons, Eq.(3.13) suggests that the transformation acting on K must have the form of a Lorentz transformation Λ . In fact, there is no room for other possibilities if the mapping is expected to change an arbitrary number of spectator momenta at the same time, preserving their onshellness. Linear as it is, the same Lorentz transformation must also act on each individual spectator:

$$K^\mu = \Lambda^\mu{}_\nu \tilde{K}^\nu, \quad (3.16)$$

$$k_i^\mu = \Lambda^\mu{}_\nu \tilde{k}_i^\nu, \quad i \in \{1, \dots, m-1\}. \quad (3.17)$$

An explicit representation of Λ is given in Ref. [43]

$$\Lambda(K, \tilde{K})^\mu{}_\nu = g^\mu{}_\nu - \frac{2(K + \tilde{K})^\mu (K + \tilde{K})_\nu}{(K + \tilde{K})^2} + \frac{2K^\mu \tilde{K}_\nu}{K^2}, \quad (3.18)$$

where

$$K = Q - P_{ij}, \quad (3.19)$$

$$\tilde{K} = Q - \tilde{p}_i. \quad (3.20)$$

Note again that, in the singular limit $P_{ij}^2 = m_i^2$, one gets $\tilde{K} = K$ and the mapping reduces to a simple identity. Incidentally, we observe that (3.18) is only one of many possible representations: indeed, any transformation $\Lambda' = \Lambda \cdot R_\alpha(\tilde{K})$, where $R_\alpha(\tilde{K})$ is a spatial

rotation of angle α around the direction of \tilde{K} , is acceptable under the condition that $\alpha \rightarrow 0$ in the singular limits.

We now turn to the case where the splitting involves an initial-state parton. We take such partons to be on-shell, massless and with zero transverse momentum,

$$p_a^2 = p_b^2 = \tilde{p}_a^2 = \tilde{p}_b^2 = 0 . \quad (3.21)$$

Let us assume that parton a splits, $\tilde{p}_a \rightarrow p_a - p_j \equiv P_{aj}$. The Nagy-Soper mapping leaves the other initial-state parton unchanged,

$$\tilde{p}_b = p_b , \quad (3.22)$$

while it acts on the final state in a way that preserves the invariant mass K^2 of the collective spectator. However, unlike the case of final-state splitting, the total momentum $Q = p_a + p_b$ is not preserved here. The additional constraint necessary to fix uniquely the $\{\tilde{p}\}_m^{(aj)}$ kinematics is given by the zero transverse momentum of the splitting parton, which implies that the momenta before and after the splitting are related by a simple rescaling:

$$\tilde{p}_a = x p_a . \quad (3.23)$$

Here the variable $x \in [0, 1]$ parameterizes the softness of the initial-state splitting, $x \rightarrow 1$ representing the soft limit. Now the momenta of the collective spectator before and after the splitting are given by

$$\tilde{K} = \tilde{p}_a + \tilde{p}_b , \quad (3.24)$$

$$K = p_a + p_b - p_j , \quad (3.25)$$

so the constraint $\tilde{K}^2 = K^2$ allows to fix the value of \tilde{p}_a through

$$x = \frac{K^2}{Q^2} . \quad (3.26)$$

As to the spectator partons, the Lorentz transformation relating momenta before and after the splitting takes again the form (3.18). Note that in the soft and collinear limits, where one can write p_j to be proportional to p_a , namely $p_j = \kappa p_a$, one has $K^2 = (1 - \kappa)Q^2$, therefore $1 - \kappa = x$ and the mapping $P_{aj} \equiv p_a - p_j \rightarrow \tilde{p}_a$ reduces to an identity.

3.3 Splitting functions

We now proceed to derive the splitting functions $\mathcal{D}^{(ijk)}(\{\tilde{p}\}_m^{ij}, \{p\}_{m+1})$ in the Nagy-Soper formalism. It is convenient to take spin correlations in evidence and rewrite Eq.(2.18) in the form

$$\mathcal{A}^D = \sum_{i,j,k=1}^{m+1} \mathcal{A}^B(\{\tilde{p}\}_m^{(ij)}) \otimes \mathcal{D}^{(ijk)}(\{\tilde{p}\}_m^{(ij)}, \{p\}_{m+1}) \quad (3.27)$$

$$= \sum_{i,j,k=1}^{m+1} \sum_{\tilde{s}_1, \tilde{s}_2 = \pm} \mathcal{A}_{\tilde{s}_1 \tilde{s}_2}^B(\{\tilde{p}\}_m^{(ij)}) \mathcal{D}_{\tilde{s}_1 \tilde{s}_2}^{(ijk)}(\{\tilde{p}\}_m^{(ij)}, \{p\}_{m+1}) (\mathbf{T}_i \cdot \mathbf{T}_k) , \quad (3.28)$$

where \tilde{s}_1, \tilde{s}_2 are the helicity values of the splitting partons \tilde{p}_i, \tilde{p}_k , while $(\mathbf{T}_i \cdot \mathbf{T}_k)$ denotes the color correlator. Note that when $i = k$, the color correlator reduces to a simple overall color factor. The function $\mathcal{D}_{\tilde{s}_1 \tilde{s}_2}^{(ijk)}$ splits into two kind of contributions $W^{(ii,j)}$ and $W^{(ik,j)}$, called respectively *diagonal* and *interference* terms:

$$\mathcal{D}_{\tilde{s}_1 \tilde{s}_2}^{(ijk)} = W_{\tilde{s}_1 \tilde{s}_2}^{(ii,j)} \delta_{ik} + W_{\tilde{s}_1 \tilde{s}_2}^{(ik,j)} (1 - \delta_{ik}) \delta_{\tilde{s}_1 \tilde{s}_2} . \quad (3.29)$$

At NLO, while the diagonal terms $W_{\tilde{s}_1 \tilde{s}_2}^{(ii,j)}$ show both soft and collinear singularities, the interference terms $W_{\tilde{s}_1 \tilde{s}_2}^{(ik,j)}$ can only be divergent in the soft limit, since the jet function excludes any configuration where partons p_i, p_k are simultaneously collinear to p_j . The factor $\delta_{\tilde{s}_1 \tilde{s}_2}$ in the interference term is justified by the fact that, in the soft limit, the two partons connected by a soft gluon exchange have the same spin index.

Let us consider a generic QCD matrix element \mathcal{M}_{m+1} characterized by $m+1$ external legs, and look at the way it factorizes when an external parton splits. We take the case of a final-state splitting as an example. Depending on flavor, there are three possible splittings: $q \rightarrow qg$, $g \rightarrow q\bar{q}$ and $g \rightarrow gg$. The corresponding matrix elements read:

$$\mathcal{M}_{m+1}^{q \rightarrow qg} = \mathcal{H}_m \frac{\not{P}_{ij} + m_i}{P_{ij}^2 - m_i^2} (\sqrt{4\pi\alpha_s} \mathbf{T}_i) \not{\epsilon}^*(p_j, s_j) u(p_i, s_i) , \quad (3.30)$$

$$\mathcal{M}_{m+1}^{g \rightarrow q\bar{q}} = \mathcal{H}_m^\mu \frac{D_{\mu\nu}(P_{ij}, n_i)}{P_{ij}^2} \bar{u}(p_j, s_j) (\sqrt{4\pi\alpha_s} \mathbf{T}_i) \gamma^\nu u(p_i, s_i) , \quad (3.31)$$

$$\mathcal{M}_{m+1}^{g \rightarrow gg} = \mathcal{H}_m^\mu \frac{D_{\mu\nu}(P_{ij}, n_i)}{P_{ij}^2} (\sqrt{4\pi\alpha_s} \mathbf{T}_i) G_{\nu\rho\sigma} \varepsilon^\rho(p_i, s_i)^* \varepsilon^\sigma(p_j, s_j)^* . \quad (3.32)$$

We generically indicate with \mathbf{T}_i the color matrix associated with the splitting $\tilde{p}_i \rightarrow p_i + p_j$. Furthermore, $\varepsilon(p, s)$ and $u(p, s)$ represent polarization vectors and spinors for a given assignment of momentum p and helicity s . \mathcal{H}_m is a m -parton subamplitude, and $G^{\nu\rho\sigma}$ denotes the triple gluon vertex

$$G^{\nu\rho\sigma} \equiv g^{\nu\rho}(p_j - p_i)^\sigma + g^{\rho\sigma}(p_i + P_{ij})^\nu + g^{\sigma\nu}(-P_{ij} - p_j)^\rho . \quad (3.33)$$

Finally, $D^{\mu\nu}$ is the numerator of the gluonic propagator in the axial gauge

$$D^{\mu\nu}(P, n) = -g^{\mu\nu} + \frac{P^\mu n^\nu + P^\nu n^\mu}{P \cdot n_i} , \quad (3.34)$$

where n_i is an arbitrary light-like vector whose definition closely follows Ref. [43]²

$$n_i \equiv \begin{cases} p_b , & \text{for } i = a , \\ p_a , & \text{for } i = b , \\ Q - \frac{Q^2}{Q \cdot \tilde{p}_i + \sqrt{(Q \cdot \tilde{p}_i)^2 - Q^2 m_i^2}} \tilde{p}_i , & \text{for } i \in \{1, \dots, m-1\} . \end{cases} \quad (3.35)$$

²In the original formulation by Nagy and Soper [43], the initial-state partonic momenta p_a, p_b appearing in Eq.(3.35) are replaced by the corresponding *hadronic* momenta, denoted p_A, p_B . We note that either choice is equivalent for the purposes of subtraction, since the vector n_i always appears in ratios, and any possible dependence upon the hadronic momentum fractions fully cancels in the end.

The subsequent step is to find out expressions which approximate the divergent behavior of Eqs.(3.30), (3.31), (3.32). One can start by inserting simple identities on the right side of the subamplitude \mathcal{H}_m :

$$1 = \frac{(\not{\tilde{p}}_i + m_i) \not{n}_i + \not{n}_i (\not{\tilde{p}}_i - m_i)}{2 \tilde{p}_i \cdot n_i}, \quad (3.36)$$

$$g^{\alpha\mu} = -D^{\alpha\mu}(\tilde{p}_i, n_i) + \frac{\tilde{p}_i^\alpha n_i^\mu + n_i^\alpha \tilde{p}_i^\mu}{\tilde{p}_i \cdot n_i}. \quad (3.37)$$

The first identity is used for the $q \rightarrow qg$ splitting, while the second one applies to the other two cases, $g \rightarrow q\bar{q}$ and $g \rightarrow gg$. We remind that \tilde{p}_i is an on-shell vector with $\tilde{p}_i^2 = p_i^2 = m_i^2$. In Ref. [43], it has been proved explicitly that the contribution coming from the second term in both identities does not lead to any collinear or soft singularity and can thus be discarded. There is a simple way of understanding this property, based on equations of motion and Ward identity. Indeed, in the singular limit $P_{ij}^2 \rightarrow m_i^2$, where $P_{ij} \approx \tilde{p}_i$, one can write

$$\not{\tilde{p}}_{ij} + m_i \approx \sum_{\tilde{s}_i=\pm} u(\tilde{p}_i, \tilde{s}_i) \bar{u}(\tilde{p}_i, \tilde{s}_i), \quad (3.38)$$

$$D^{\alpha\mu}(P_{ij}, n_i) \approx \sum_{\tilde{s}_i=\pm} \varepsilon^\alpha(\tilde{p}_i, \tilde{s}_i)^* \varepsilon^\mu(\tilde{p}_i, \tilde{s}_i). \quad (3.39)$$

It immediately follows that the second term in (3.36) gives a vanishing contribution due to the equation of motion $(\not{\tilde{p}}_i - m_i) u(\tilde{p}_i, \tilde{s}_i) = 0$. Similarly, the second term in (3.37) vanishes thanks to Ward identity, $\tilde{p}_i^\mu \mathcal{H}_\mu = 0$. Note that $n_i^\mu \mathcal{H}_\mu = 0$ in the axial gauge we are considering.

Neglecting the second term from the identities, one is left with the following expressions which approximate the divergent behavior of the original matrix elements:

$$\mathcal{M}_{m+1}^{q \rightarrow qg, div} = \mathcal{H}_m \frac{(\not{\tilde{p}}_i + m_i) \not{n}_i}{2 \tilde{p}_i \cdot n_i} \frac{\not{\tilde{p}}_{ij} + m_i}{P_{ij}^2 - m_i^2} (\sqrt{4\pi\alpha_s} \mathbf{T}_i) \not{\epsilon}^*(p_j, s_j) u(p_i, s_i), \quad (3.40)$$

$$\mathcal{M}_{m+1}^{g \rightarrow q\bar{q}, div} = -\mathcal{H}_m^\alpha D_{\alpha\mu}(\tilde{p}_i, n_i) \frac{D^{\mu\nu}(P_{ij}, n_i)}{P_{ij}^2} \bar{u}(p_j, s_j) (\sqrt{4\pi\alpha_s} \mathbf{T}_i) \gamma^\nu u(p_i, s_i), \quad (3.41)$$

$$\mathcal{M}_{m+1}^{g \rightarrow gg, div} = \mathcal{H}_m^\alpha D_{\alpha\mu}(\tilde{p}_i, n_i) \frac{D^{\mu\nu}(P_{ij}, n_i)}{P_{ij}^2} (\sqrt{4\pi\alpha_s} \mathbf{T}_i) G_{\nu\rho\sigma} \varepsilon^\rho(p_i, s_i)^* \varepsilon^\sigma(p_j, s_j)^* \quad (3.42)$$

Now using

$$\not{\tilde{p}}_i + m_i = \sum_{\tilde{s}_i=\pm} u(\tilde{p}_i, \tilde{s}_i) \bar{u}(\tilde{p}_i, \tilde{s}_i), \quad (3.43)$$

$$D^{\alpha\mu}(\tilde{p}_i, n_i) = \sum_{\tilde{s}_i=\pm} \varepsilon^\alpha(\tilde{p}_i, \tilde{s}_i)^* \varepsilon^\mu(\tilde{p}_i, \tilde{s}_i), \quad (3.44)$$

and associating the first factor in (3.43), (3.44) with the subamplitude \mathcal{H}_m , one gets a product of a complete m -parton scattering amplitude times a genuine splitting function,

i.e. $\mathcal{M}_{m+1}^{div} = \mathcal{H}_m \otimes v$. Once the contribution of color degrees of freedom is factored out, the splitting functions take the final form:

$$v_{\tilde{s}_i s_i s_j}^{(ij)}(q \rightarrow qg) = \frac{\sqrt{4\pi\alpha_s}}{P_{ij}^2 - m_i^2} \frac{\bar{u}(\tilde{p}_i, \tilde{s}_i) \not{n}_i (\not{P}_{ij} + m_i) \not{\epsilon}(p_j, s_j) u(p_i, s_i)}{2\tilde{p}_i \cdot n_i}, \quad (3.45)$$

$$v_{\tilde{s}_i s_i s_j}^{(ij)}(g \rightarrow q\bar{q}) = -\frac{\sqrt{4\pi\alpha_s}}{P_{ij}^2} \varepsilon^\mu(\tilde{p}_i, \tilde{s}_i) D_{\mu\nu}(P_{ij}, n_i) \bar{u}(p_j, s_j) \gamma^\nu u(p_i, s_i), \quad (3.46)$$

$$v_{\tilde{s}_i s_i s_j}^{(ij)}(g \rightarrow gg) = \frac{\sqrt{4\pi\alpha_s}}{P_{ij}^2} D^{\mu\nu}(P_{ij}, n_i) G_{\nu\rho\sigma} \varepsilon_\mu(\tilde{p}_i, \tilde{s}_i) \varepsilon^\rho(p_i, s_i)^* \varepsilon^\sigma(p_j, s_j)^*. \quad (3.47)$$

Note that functions (3.45) and (3.47) show both collinear and soft divergences, whereas in the case of $g \rightarrow q\bar{q}$ splitting, Eq.(3.46), the divergence can only be collinear. In all cases where the splitting functions reach the soft limit, gluon emission can be treated in the eikonal approximation, and the splitting function reduces to a much simpler expression:

$$v_{\tilde{s}_i s_i s_j}^{(ij), eik} = \sqrt{4\pi\alpha_s} \delta_{\tilde{s}_i, s_i} \frac{\varepsilon(p_j, s_j)^* \cdot p_i}{p_i \cdot p_j}. \quad (3.48)$$

The derivation of the splitting functions in the case of initial-state radiation is quite similar, the only formal difference being in the form of the spinors and polarization vectors, and possibly in an overall sign. A comprehensive list of splitting functions, including the case of initial-state emission, is reported in Ref. [43].

In the last step, the splitting functions are combined to give the diagonal and interference contributions to the dipole $\mathcal{D}_{\tilde{s}_1 \tilde{s}_2}^{(ijk)}$ as to Eq.(3.29):

$$W_{\tilde{s}_1 \tilde{s}_2}^{(ii,j)} = \sum_{s_i, s_j} v_{\tilde{s}_1 s_i s_j}^{(ij)} \left(v_{\tilde{s}_2 s_i s_j}^{(ij)} \right)^* \quad (3.49)$$

$$W_{\tilde{s}_1 \tilde{s}_2}^{(ik,j)} = \sum_{s_i, s_j} v_{\tilde{s}_1 s_i s_j}^{(ij), eik} \left(v_{\tilde{s}_2 s_i s_j}^{(kj), eik} \right)^* \delta_{\tilde{s}_1 \tilde{s}_2}. \quad (3.50)$$

Note that there is an ambiguity with the definition of the interference term $W^{(ik,j)}$, in that one can adopt either the mapping $\{\tilde{p}\}_m^{(ij)}$ or $\{\tilde{p}\}_m^{(kj)}$ to compute it. Instead of choosing one, it is also possible to take a weighted combination of the two:

$$W^{(ik,j)} = A_{ik} W_{[i]}^{(ik,j)} + A_{ki} W_{[k]}^{(ik,j)}. \quad (3.51)$$

Here the subscript $[i]$ ($[k]$) means that the corresponding term is evaluated considering the mapping $\{\tilde{p}\}_m^{(ij)}$ ($\{\tilde{p}\}_m^{(kj)}$). The weight factors always satisfy the condition

$$A_{ik} + A_{ki} = 1. \quad (3.52)$$

One motivation for taking such a combination, as discussed in detail in [44, 45], is that it shows more favorable properties in the context of the parton shower. Including the color factor, the net contribution summed over the two graphs arising from the interference of soft gluons emitted from partons i and k is

$$W^{(ik,j)}(\mathbf{T}_i \cdot \mathbf{T}_k) + W^{(ki,j)}(\mathbf{T}_k \cdot \mathbf{T}_i) \quad (3.53)$$

$$= A_{ik} \left[W_{[i]}^{(ik,i)}(\mathbf{T}_i \cdot \mathbf{T}_k) + W_{[i]}^{(ki,j)}(\mathbf{T}_k \cdot \mathbf{T}_i) \right] \quad (3.54)$$

$$+ A_{ki} \left[W_{[k]}^{(ik,i)}(\mathbf{T}_i \cdot \mathbf{T}_k) + W_{[k]}^{(ki,j)}(\mathbf{T}_k \cdot \mathbf{T}_i) \right]. \quad (3.55)$$

Note that the weight factors can be either constants or functions of $\{p\}_{m+1}$. Several expressions for them have been proposed in the literature. In our implementation, we consider the definition given by Eq.(7.12) of Ref. [45]:

$$A_{ik} = \frac{(p_j \cdot p_k)(p_i \cdot Q)}{(p_j \cdot p_k)(p_i \cdot Q) + (p_i \cdot p_j)(p_k \cdot Q)}. \quad (3.56)$$

3.4 Phase space factorization

An important feature of the Nagy-Soper mapping is that all spectator momenta are changed at the same time. This fact obviously has an impact on the way the factorization of the phase space is achieved. While in the case of initial-state emission there are no substantial differences with respect to the Catani-Seymour scheme, the factorization is derived in a slightly different way when the splitting occurs in the final state. Let us start with the usual definition of the Lorentz invariant phase space for a generic final state with $m + 1$ partons, where we closely follow the notation introduced in Section 3.1:

$$d\Phi_{m+1}(p_i, p_j, k_1, \dots, k_{m-1}; Q) \equiv \quad (3.57)$$

$$\frac{d^3 p_i}{(2\pi)^d 2p_i^0} \frac{d^3 p_j}{(2\pi)^d 2p_j^0} \frac{d^3 k_1}{(2\pi)^d 2k_1^0} \dots \frac{d^3 k_{m-1}}{(2\pi)^d 2k_{m-1}^0} (2\pi)^d \delta^d(Q - p_i - p_j - k_1 - \dots - k_{m-1}).$$

We re-organize the phase space in terms of recursive splittings, as schematically represented in Fig.1:

$$d\Phi_{m+1}(p_i, p_j, k_1, \dots, k_m; Q) = \quad (3.58)$$

$$\int_{K_{min}^2}^{K_{max}^2} \frac{dK^2}{2\pi} \int_{P_{min}^2}^{P_{max}^2} \frac{dP_{ij}^2}{2\pi} d\Phi_{m-1}(k_1, \dots, k_{m-1}; K) d\Phi_2(P_{ij}, K; Q) d\Phi_2(p_i, p_j; P_{ij}),$$

where

$$K_{min}^2 = (m_{k_1} + \dots + m_{k_{m-1}})^2 \quad (3.59)$$

$$K_{max}^2 = (\sqrt{Q^2} - m_{p_i} - m_{p_j})^2 \quad (3.60)$$

$$P_{min}^2 = (m_{p_i} + m_{p_j})^2 \quad (3.61)$$

$$P_{max}^2 = (\sqrt{Q^2} - \sqrt{K^2})^2. \quad (3.62)$$

Here $m_{p_i}, m_{p_j}, m_{k_i}$ represent the masses of the on-shell final-state partons, while $\sqrt{K^2}$ is the invariant mass of the collective spectator. Looking at the first factor in the integral (3.58), one observes that

$$d\Phi_{m-1}(k_1, \dots, k_{m-1}; K) = d\Phi_{m-1}(\tilde{k}_1, \dots, \tilde{k}_{m-1}; \tilde{K}). \quad (3.63)$$

This immediately follows from the fact that the mapping $K \rightarrow \tilde{K}$ is a Lorentz transformation, and the phase space is Lorentz invariant. The Jacobian of the second factor is not as trivial, but admits a simple derivation in the frame where the total momentum Q is at rest. In this frame, the two-body phase space can be parameterized in terms of angular variables,

$$d\Phi_2(P_{ij}, K; Q) = \frac{1}{8(2\pi)^{d-2}} \frac{\lambda(Q^2, P_{ij}^2, K^2)^{\frac{d-3}{2}}}{(Q^2)^{\frac{d-2}{2}}} \int d\Omega_{d-1}, \quad (3.64)$$

where $d\Omega_{d-1}$ represents the solid angle in d dimensions and λ is the standard Källén function,

$$\lambda(x, y, z) = x^2 + y^2 + z^2 - 2xy - 2xz - 2yz. \quad (3.65)$$

It should be clear from Eq.(3.11) that, when the total momentum Q is at rest, the vector \vec{p}_i is just proportional to \vec{P}_{ij} . Thus, the two spatial vectors are described by the same angular variables, and the integral $\int d\Omega_{d-1}$ for the two phase spaces $d\Phi_2(P_{ij}, K; Q)$ and $d\Phi_2(\tilde{p}_i, \tilde{K}; Q)$ is the same. This implies that the Jacobian related to the mapping $P_{ij} \rightarrow \tilde{p}_i$ is simply

$$d\Phi_2(P_{ij}, K; Q) = \left(\frac{\lambda(Q^2, P_{ij}^2, K^2)}{\lambda(Q^2, m_i^2, K^2)} \right)^{\frac{d-3}{2}} d\Phi_2(\tilde{p}_i, \tilde{K}; Q). \quad (3.66)$$

In the end, the phase space for the final-state emission can be expressed in the fully factorized form

$$d\Phi_{m+1}(p_i, p_j, k_1, \dots, k_{m-1}; Q) = d\Phi_m(\tilde{p}_i, \tilde{k}_1, \dots, \tilde{k}_{m-1}; Q) \times d\xi_{fin}, \quad (3.67)$$

where

$$d\xi_{fin} = \frac{dP_{ij}^2}{2\pi} \left(\frac{\lambda(Q^2, P_{ij}^2, K^2)}{\lambda(Q^2, m_i^2, K^2)} \right)^{\frac{d-3}{2}} d\Phi_2(p_i, p_j; \underbrace{\beta \tilde{p}_i + \gamma Q}_{P_{ij}}) \quad (3.68)$$

is the measure of the splitting phase space in d dimensions.

As already mentioned, in the case of initial-state emission, the factorization of the phase space does not show conceptual differences with Catani-Seymour subtraction, where the splitting phase space is written as [42]

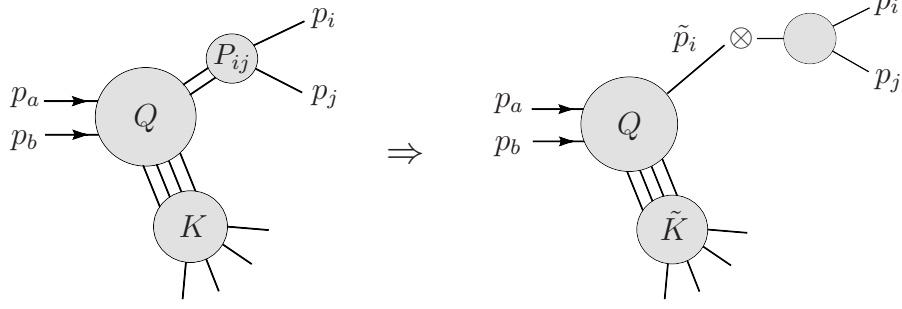
$$d\xi_{ini} = \frac{d^{d-1}p_j}{(2\pi)^{d-1} 2p_j^0} \Theta(x)\Theta(1-x) \delta(x - \bar{x}(p_j)). \quad (3.69)$$

The variable x appearing in the formula is the same defined in Eq.(3.23), $\tilde{p}_a = xp_a$, namely the one that parameterizes the softness of the initial-state radiation. The factor $\delta(x - \bar{x}(p_j))$ comes from the fact that the value of x is dictated by the kinematics of the unconstrained parton p_j and can thus be expressed as a function of it, $\bar{x}(p_j)$. The explicit form of the integration measures, Eqs.(3.68)-(3.69), obviously depends on the specific parameterization of the phase space and will be clear in Section 4.1, where we define the splitting variables used in our calculation.

4 Integration over the unresolved phase space

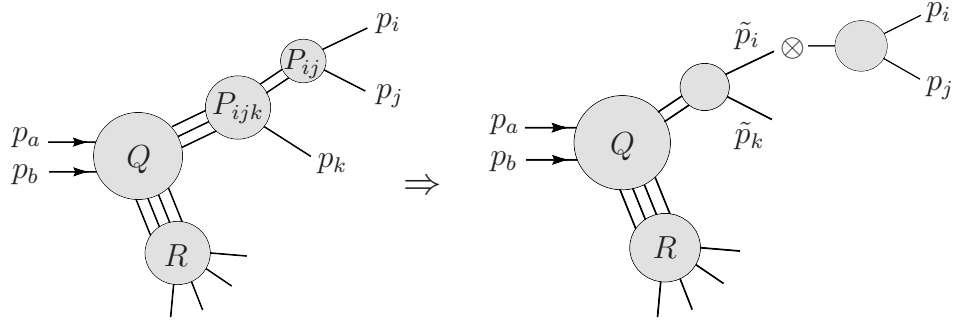
4.1 Splitting variables

In $d = 4$ dimensions, the phase space of the splitting has three degrees of freedom. One possible way of parameterizing them relies on scalar products and splitting variables defined in a Lorentz-covariant fashion, as proposed in Ref. [46]. In fact, this choice is conceptually simple and leads to quite compact formulae of the integrated dipoles for massless partons [47]. On the other hand, when one turns to the fully massive case, the kinematical bounds



$$\{p_i, p_j\} \rightarrow \tilde{p}_i ; \{K, Q\} \rightarrow \{\tilde{K}, Q\}$$

$$p_i + p_j + K = \tilde{p}_i + \tilde{K}$$



$$\{p_i, p_j\} \rightarrow \tilde{p}_i ; \{p_k, R, Q\} \rightarrow \{\tilde{p}_k, R, Q\}$$

$$p_i + p_j + p_k = \tilde{p}_i + \tilde{p}_k$$

Figure 1. Schematic representation of the phase space factorization and parameterization in terms of recursive splittings: comparison between the Nagy-Soper scheme (top) and the Catani-Seymour scheme (bottom). p_i and p_j are the splitting momenta, whereas the remaining momenta are classified as spectators. The shown example refers to the case of a final-state splitting.

of the splitting get more complicated and many additional terms are generated in the formulae. With the goal of keeping the final expressions reasonably compact, which we find desirable for our semi-numerical approach, we have adopted an alternative parameterization that we describe in this Section.

Let us start with the case of a final-state emission. Given a set of momenta $\{\tilde{p}\}_m$ as input, we want to construct the splitting $\tilde{p}_i \rightarrow p_i + p_j$ and thus the set of momenta $\{p\}_{m+1}$ out of three parameters that we call *collinear*, *soft* and *azimuthal* variables. In the singular limit $P_{ij}^2 \rightarrow m_i^2$, the collinear and the soft variables must resemble the two quantities that naturally parameterize the collinearity and softness of the splitting, *i.e.* the relative angle between the nearly-collinear partons, θ_{ij} , and the energy of the unresolved parton, E_j . By azimuthal variable, we mean the second angular parameter that is necessary in order to

uniquely fix the kinematics of the splitting.

The definition of the angular variables requires a reference frame to be set. We consider an orthogonal set of axes (x, y, z) , and identify the z -axis with the spatial direction of the vector \tilde{p}_i . There is full freedom in selecting the direction of the x -axis: when this is done, the azimuthal variable is uniquely determined as the angle ϕ_j which separates the unresolved parton p_j from the the x - z plane. A convenient choice is to consider the spectator momentum \tilde{p}_k which appears in each interference term as a reference direction, so that the x -axis lies on the plane \tilde{p}_i - \tilde{p}_k as shown in Figure 2. This choice obviously helps to keep the dependence of the integrands upon the azimuthal variable as simple as possible. In this frame, the angle θ_j between partons p_j and \tilde{p}_i is a good candidate for the collinear variable. Note that when $P_{ij}^2 \approx m_i^2$, one gets indeed $\tilde{p}_i \approx p_i + p_j$ and thus $\cos \theta_j \approx \cos \theta_{ij}$. The definition of the soft variable is more complicated, since the relation between the energy E_j and the invariant mass P_{ij}^2 is not generally invertible. In the Lorentz frame where the total momentum Q is at rest, it reads

$$E_j = \frac{\sqrt{Q^2} (P_{ij}^2 - m_i^2)}{P_{ij}^2 - m_i^2 + 2 \sqrt{Q^2} (\tilde{p}_i^0 - \cos \theta_j \beta |\vec{p}_i|)} . \quad (4.1)$$

The parameter β is given by Eq.(3.14) and is a non-monotonic function of P_{ij}^2 . In consequence, by choosing E_j as the soft variable, one would be led to some ambiguity in the assignment of P_{ij}^2 . We observe, however, that such ambiguity is solved if one sets $\beta = 1$ in (4.1). In fact, this defines a new variable \bar{E}_j :

$$\bar{E}_j \equiv \frac{\sqrt{Q^2} (P_{ij}^2 - m_i^2)}{P_{ij}^2 - m_i^2 + 2 \sqrt{Q^2} (\tilde{p}_i^0 - \cos \theta_j |\vec{p}_i|)} . \quad (4.2)$$

Clearly when $P_{ij}^2 \approx m_i^2$ one has $\beta \approx 1$ and therefore $\bar{E}_j \approx E_j$, hence the variable \bar{E}_j is a good candidate to be a soft variable. It is further convenient to divide it by its kinematically allowed maximum value and get a normalized soft variable e :

$$e \equiv \bar{E}_j / \bar{E}_j^{max} , \quad (4.3)$$

where

$$\bar{E}_j^{max} = \frac{\sqrt{Q^2} (P_{ij,max}^2 - m_i^2)}{P_{ij,max}^2 - m_i^2 + 2 \sqrt{Q^2} (\tilde{p}_i^0 - \cos \theta_j |\vec{p}_i|)} , \quad (4.4)$$

and $P_{ij,max}^2$ is given by Eq.(3.62). To summarize, in case of final-state emission, the integration of the splitting phase space runs over the variables

$$e \in [0, 1] , \quad (4.5)$$

$$c \equiv \cos \theta_j \in [-1, 1] \quad (4.6)$$

$$\phi \equiv \phi_j \in [0, 2\pi] . \quad (4.7)$$

The soft and collinear limits correspond to $e \rightarrow 0$ and $c \rightarrow 1$ respectively.

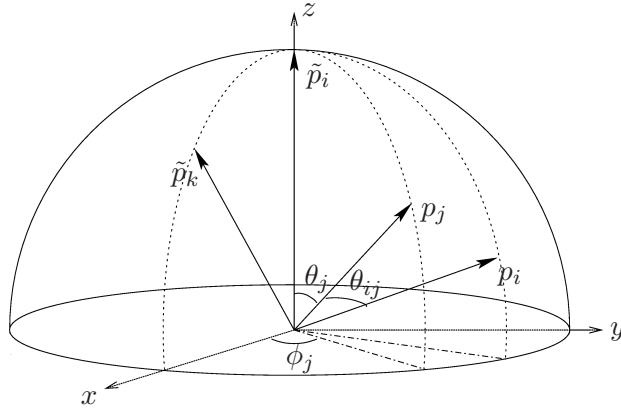


Figure 2. Parameterization of the angular variables for the final-state splitting $\tilde{p}_i \rightarrow p_i + p_j$. Here \tilde{p}_k is the spectator parton selected to define the azimuthal variable ϕ_j .

In the case of initial-state splitting, the kinematics is simpler and the choice of the splitting variables is more straightforward. We consider

$$\tilde{p}_a = x p_a \quad (4.8)$$

$$\tilde{p}_b = p_b \quad (4.9)$$

and we take x to be our soft variable, the soft limit being $x \rightarrow 1$. In the frame where the total momentum *before* the splitting, $Q = p_a + p_b$, is at rest, the relation between E_j and x is particularly simple:

$$E_j = \frac{1}{2} \sqrt{Q^2} (1 - x). \quad (4.10)$$

Note that $Q^2 = \tilde{K}^2/x$, where $\tilde{K} = \tilde{p}_a + \tilde{p}_b$. We build our reference frame by identifying the z -axis with the vector \tilde{p}_a , and select one spectator parton \tilde{p}_k so that the plane \tilde{p}_a - \tilde{p}_k defines the azimuthal variable ϕ_j . Finally, the angle between parton p_j and the beam axis defines the collinear variable θ_j as shown in Figure 3. The integration of the splitting phase space runs in the case of initial-state emission over the variables

$$x \in [0, 1], \quad (4.11)$$

$$c \equiv \cos \theta_j \in [-1, 1], \quad (4.12)$$

$$\phi \equiv \phi_j \in [0, 2\pi]. \quad (4.13)$$

The soft and collinear limits correspond to $x \rightarrow 1$ and $c \rightarrow 1$ respectively.

4.2 Semi-numerical approach

For the calculation of the integrated subtraction terms, we adopt the spin-averaged version of the splitting functions described in Ref. [44]. In $d = 4 - 2\epsilon$ dimensions, one has:

$$\overline{W}^{(ii,j)} = F_i \sum_{\tilde{s}_i = \pm} W_{\tilde{s}_i, \tilde{s}_i}^{(ii,j)} \quad (4.14)$$

$$\overline{W}^{(ik,j)} = \frac{1}{2(1-\epsilon)} \sum_{\tilde{s}_i = \pm} W_{\tilde{s}_i, \tilde{s}_i}^{(ik,j)}. \quad (4.15)$$

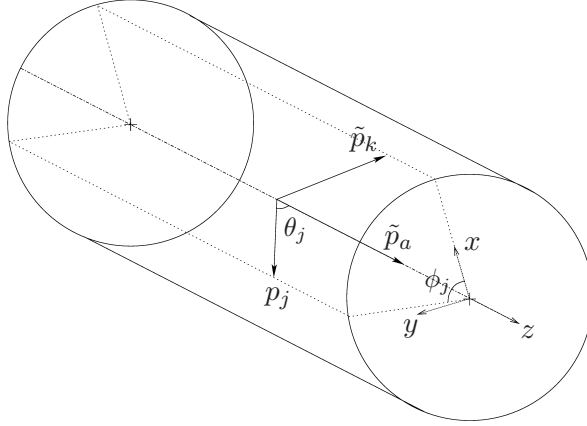


Figure 3. Parameterization of the angular variables for the initial-state splitting $\tilde{p}_a \rightarrow p_a + p_j$. Here \tilde{p}_k is the spectator parton selected to define the azimuthal variable ϕ_j .

The average factor F_i takes the value $1/2$ if the splitting parton \tilde{p}_i is a quark, and $1/(2(1-\epsilon))$ if it is a gluon. Including the color operator and exploiting the invariance of the matrix element under color rotations,

$$(\mathbf{T}_i \cdot \mathbf{T}_i) = - \sum_{k \neq i} \frac{1}{2} [(\mathbf{T}_i \cdot \mathbf{T}_k) + (\mathbf{T}_k \cdot \mathbf{T}_i)] , \quad (4.16)$$

one can arrange the full integrand for a given mapping $\{\tilde{p}\}_m^{(ij)}$ in the form

$$\frac{1}{2} [(\mathbf{T}_i \cdot \mathbf{T}_k) + (\mathbf{T}_k \cdot \mathbf{T}_i)] [\overline{W}^{(ii,j)} - \overline{W}^{(ik,j)}] . \quad (4.17)$$

Following [44], we further split the integrand $[\overline{W}^{(ii,j)} - \overline{W}^{(ik,j)}]$ into two pieces,

$$\overline{W}^{(ii,j)} - \overline{W}^{(ik,j)} = \underbrace{(\overline{W}^{(ii,j)} - \overline{W}^{(ii,j),eik})}_{\mathcal{D}_{ii}} + \underbrace{(\overline{W}^{(ii,j),eik} - \overline{W}^{(ik,j)})}_{\mathcal{I}_{ik}} , \quad (4.18)$$

where $\overline{W}^{(ii,j),eik}$ is based on the eikonal approximation (3.48). This splitting has the advantage that the first term, \mathcal{D}_{ii} , can only have a collinear singularity by construction, while the second term, \mathcal{I}_{ik} , can be both soft- and collinear-divergent. On the other hand, the latter can be expressed in the simple universal form [44]

$$\mathcal{I}_{ik} = 4\pi\alpha_s A_{ik} \frac{-((p_j \cdot p_k) p_i - (p_i \cdot p_j) p_k)^2}{(p_i \cdot p_j)^2 (p_j \cdot p_k)^2} . \quad (4.19)$$

Our goal is to integrate (4.18) over the whole phase space of the splitting. For clarity, we will present the cases of initial- and final-state emission separately. It is convenient to make explicit reference to our splitting variables, defined in Section 4.1, and write the

integrated subtraction terms as follows:

$$D_{ii} \equiv \int d\xi_{fin}^d \mathcal{D}_{ii}^d = \int de dc d\phi J_{fin}^d(e, c, \phi) \mathcal{D}_{ii}^d(e, c, \phi) , \quad (4.20)$$

$$I_{ik} \equiv \int d\xi_{fin}^d \mathcal{I}_{ik}^d = \int de dc d\phi J_{fin}^d(e, c, \phi) \mathcal{I}_{ik}^d(e, c, \phi) , \quad (4.21)$$

$$D_{aa}(\cdot) \equiv \int d\xi_{ini}^d \mathcal{D}_{aa}^d = \int dx dc d\phi J_{ini}^d(x, c, \phi) \mathcal{D}_{aa}^d(x, c, \phi) , \quad (4.22)$$

$$I_{ak}(\cdot) \equiv \int d\xi_{ini}^d \mathcal{I}_{ak}^d = \int dx dc d\phi J_{ini}^d(x, c, \phi) \mathcal{I}_{ak}^d(x, c, \phi) . \quad (4.23)$$

Here, the superscript d means that the corresponding quantity is evaluated in d space-time dimensions, while J^d represents the Jacobian of the phase space measure associated with our splitting variables. When the splitting involves an initial-state parton, we use the symbol " (\cdot) " to clarify that the integrated term is a distribution in the x variable, thus the corresponding integral is well defined only in a convolution with some test function $f(x)$.

It has been already pointed out that, in consequence of the increased complexity of the mapping, a fully analytic evaluation of the integrals (4.20), (4.21), (4.22), (4.23) is challenging in the Nagy-Soper scheme. A viable alternative is to use numerical approaches, such as Gaussian integration or Monte Carlo, to integrate over the splitting phase space. Given the general complexity of the integrands, we decided to adopt a *semi-numerical* approach, namely to consider analytic integration when possible, and Monte Carlo integration otherwise. A crucial observation is that the general dependence of the integrands upon the azimuthal variable ϕ is simple. In fact, up to $\mathcal{O}(\epsilon^0)$, all the azimuthal integrals can be classified into three groups:

$$\int_0^{2\pi} d\phi \frac{1}{x + y \cos \phi} = \frac{2\pi}{\sqrt{x^2 - y^2}} \text{sign}(x) , \quad (4.24)$$

$$\int_0^{2\pi} d\phi \frac{\log(\sin^2 \phi)}{x + y \cos \phi} = \frac{4\pi}{\sqrt{x^2 - y^2}} \log \left(\frac{2\sqrt{x^2 - y^2}}{2x + \sqrt{x^2 - y^2}} \right) , \quad (4.25)$$

$$\int_0^{2\pi} d\phi \log^2(\sin^2 \phi) = \frac{2\pi^3}{3} + 2\pi \log^2(4) . \quad (4.26)$$

Here x, y denote generic real parameters. The dependence on the soft and collinear variables is not as simple and leads to more complicated expressions that deserve a numerical treatment. As an example, we will illustrate the case of the integrals (4.21) and (4.23) in the case where the emitting parton is massless. We highlight these cases because they exhibit some complication compared to other integrals, helping us to explain our approach in its most general form.

Let us start with the case of final-state interference, Eq.(4.21). After the azimuthal variable has been integrated out, one is left with a new integrand function $\mathcal{F}_{ik}^d(e, c)$ which is divergent in proximity of the soft ($e \rightarrow 0$) and/or collinear ($c \rightarrow 1$) limit. Its divergent structure is known from QCD and allows us to write,

$$\mathcal{F}_{ik}^{d=4-2\epsilon}(e, c) = \frac{\mathcal{N}_{ik}^{d=4-2\epsilon}(e, c)}{(1-c)^{1+\epsilon} e^{1+2\epsilon}} , \quad (4.27)$$

where the numerator $\mathcal{N}(e, c)_{ik}^{d=4}$ is a regular function in the full domain. Using dimensional regularization, $d = 4 - 2\epsilon$, one converts the singular structure that appears implicitly at the integrand level in the form of explicit $1/\epsilon$ and $1/\epsilon^2$ poles. To facilitate the pole extraction, we add and subtract divergent counterterms to the original integral as follows:

$$I_{ik} = \int de dc \mathcal{F}_{ik}^{d=4-2\epsilon}(e, c) \quad (4.28)$$

$$= \int de dc \frac{1}{(1-c)e} \left[\mathcal{N}_{ik}^{d=4}(e, c) - \mathcal{N}_{ik}^{d=4}(0, c) - \mathcal{N}_{ik}^{d=4}(e, 1) + \mathcal{N}_{ik}^{d=4}(0, 1) \right] \quad (4.29)$$

$$+ \int de dc \frac{1}{(1-c)^{1+\epsilon} e^{1+2\epsilon}} \left[\mathcal{N}_{ik}^{d=4-2\epsilon}(0, c) - \mathcal{N}_{ik}^{d=4-2\epsilon}(0, 1) \right] \quad (4.30)$$

$$+ \int de dc \frac{1}{(1-c)^{1+\epsilon} e^{1+2\epsilon}} \left[\mathcal{N}_{ik}^{d=4-2\epsilon}(e, 1) - \mathcal{N}_{ik}^{d=4-2\epsilon}(0, 1) \right] \quad (4.31)$$

$$+ \int de dc \frac{1}{(1-c)^{1+\epsilon} e^{1+2\epsilon}} \mathcal{N}_{ik}^{d=4-2\epsilon}(0, 1). \quad (4.32)$$

Now the integral (4.29) is convergent by construction and can be solved numerically in $d = 4$ dimensions. The full singular structure is entailed in (4.30), (4.31), (4.32) and can be directly extracted by expanding the integrand in powers of ϵ . Thus, from (4.30) and (4.31) one gets $1/\epsilon$ poles related to soft and collinear singularities, while the soft-collinear $1/\epsilon^2$ pole is a genuine contribution of (4.32). After expansion, the result is cast in the form

$$I_{ik} = \frac{1}{\epsilon^2} G_{ik}^{(2)} + \frac{1}{\epsilon} \int de dc \mathcal{G}_{ik}^{(1)}(e, c) + \int de dc \mathcal{G}_{ik}^{(0)}(e, c) \quad (4.33)$$

$$= \frac{1}{\epsilon^2} G_{ik}^{(2)} + \frac{1}{\epsilon} G_{ik}^{(1)} + \int de dc \mathcal{G}_{ik}^{(0)}(e, c). \quad (4.34)$$

Note that this is a two-dimensional application of the well-known relation

$$\frac{1}{(1-z)^{1+\epsilon}} = -\frac{1}{\epsilon} \delta(1-z) + \left(\frac{1}{1-z} \right)_+ + \dots \quad (4.35)$$

The coefficients of the poles are integrals that are simple enough to be performed fully analytically, while the finite part is left to Monte Carlo, improved with stratified sampling [72]. Both divergent and finite pieces are incorporated into the $\mathbf{I}(\epsilon)$ operator.

Let us now turn to the case of initial-state interference, Eq.(4.23). We consider a generic test function $f(x)$ in convolution with the integrated subtraction term, and rewrite the latter in the standard form

$$\begin{aligned} I_{ak}(f) &= \int dx dc f(x) \mathcal{F}_{ak}^d(x, c) \\ &= \int dx dc \left[f(x) \mathcal{F}_{ak}^d(x, c) - f(1) \mathcal{F}_{ak}^d(x, c) \right] + \int dx dc f(1) \mathcal{F}_{ak}^d(x, c) \end{aligned} \quad (4.36)$$

$$= \int dx dc f(x) \left(\mathcal{F}_{ak}^d(x, c) \right)_+ + f(1) \int dx dc \mathcal{F}_{ak}^d(x, c) \quad (4.37)$$

$$\equiv \int dx f(x) \left[\left(U_{ak}^d(x) \right)_+ + \delta(1-x) V_{ak}^d \right], \quad (4.38)$$

where $(U_{ak}^d(x))_+$ and $V_{ak}^d(x)$ are fully integrated over the collinear variable c :

$$(U_{ak}^d(x))_+ = \int dc (F_{ak}^d(x, c))_+, \quad (4.39)$$

$$V_{ak} = \int dx dc \mathcal{F}_{ak}^d(x, c). \quad (4.40)$$

As in the previous example, one can write

$$\mathcal{F}_{ak}^{d=4-2\epsilon}(x, c) = \frac{\mathcal{N}_{ak}^{d=4-2\epsilon}(x, c)}{(1-c)^{1+\epsilon}(1-x)^{1+2\epsilon}}, \quad (4.41)$$

where the numerator function is finite in the full domain. The pole structure of $(U_{ak}^d(x))_+$ and $V_{ak}^d(x)$ can now be extracted using the outlined subtraction method. As to the first element, only a collinear divergence is allowed and the subtraction procedure is simplified:

$$(U_{ak}^d(x))_+ = \int dc \left(\frac{1}{(1-c)(1-x)} \left[\mathcal{N}_{ak}^{d=4}(x, c) - \mathcal{N}_{ak}^{d=4}(x, 1) \right] \right)_+ \quad (4.42)$$

$$+ \int dc \left(\frac{1}{(1-c)^{1+\epsilon}(1-x)^{1+2\epsilon}} \mathcal{N}_{ak}^{d=4-2\epsilon}(x, 1) \right)_+ \quad (4.43)$$

In the second case, V_{ak} , both collinear and soft singularities are allowed and the procedure is the same as the one described in Eq.(4.28). Expanding the integrands in powers of ϵ , the results are finally cast in the form

$$(U_{ak}^d(x))_+ = \frac{1}{\epsilon} (K_{ak}^{(1)}(x))_+ + \int dc (\mathcal{K}_{ak}^{(0)}(x, c))_+, \quad (4.44)$$

$$V_{ak} = \frac{1}{\epsilon^2} G_{ak}^{(2)} + \frac{1}{\epsilon} G_{ak}^{(1)} + \int dx dc \mathcal{G}_{ak}^{(0)}(x, c). \quad (4.45)$$

The singular part of V_{ak} is incorporated into the $\mathbf{I}(\epsilon)$ operator. Note that the single pole of $(U_{ak}^d(x))_+$ is canceled by the corresponding singularity arising from the collinear counterterm \mathcal{A}^C , namely it is absorbed into a re-definition of the parton distribution functions. The finite pieces of both $U_{ak}(x)$ and V_{ak} are all implemented in the \mathbf{KP} operator. We stress that splitting an x -independent finite piece between the \mathbf{I} and the (x -dependent) \mathbf{KP} operator is a totally arbitrary operation, provided one casts them in the form of $\delta(1-x)$ contributions.

5 Implementation in HELAC-DIPOLES

HELAC-DIPOLES is a general purpose package for the evaluation of the real emission corrections at next-to-leading order in QCD. Based on the framework of HELAC-PHEGAS [53–56], it has been originally built using a modified version of the Catani-Seymour dipoles which applies to arbitrary helicity eigenstates of the splitting partons [50]. The package has been used together with HELAC-1LOOP [30, 32, 33, 57], CUTTOOLS [58–60] and ONELOOP [61] in the computation of full QCD corrections to several $2 \rightarrow 4$ processes at the LHC and the Tevatron [4, 6, 9, 13, 16, 18, 23].

The structure of the calculation closely follows the general discussion of Section 2. Following Eqs.(2.19-2.21), the final output obtainable from the code consists of three contributions evaluated separately³: the subtracted real part, the **I** operator and the **KP** operator contributions. Although the three terms are individually dependent on the subtraction scheme employed, their sum is independent and can be used in order to cross-check our implementation against Catani-Seymour results.

In the present extension, we have incorporated the new subtraction method based on the Nagy-Soper formalism preserving at the same time all the optimizations available in the code. For a detailed description of the package functionalities, we refer to the existing literature [33, 50]. We emphasize that all those elements of the calculation that are inherent to subtraction, but not dependent on a specific scheme, do not require to be implemented again: for example, the Born matrix elements and the color correlators are already provided by the framework of HELAC-DIPOLES. This fact dramatically simplifies our implementation.

The construction of the Nagy-Soper subtraction terms is dictated by the form of the splitting functions introduced in Section 3.3, see for instance Eqs.(3.45)-(3.47). An interesting feature of these functions is that they contain generic spinors and polarization vectors, which enables them to treat simultaneously fixed helicities as well as random polarization states. For comparison, the Catani-Seymour dipoles as to our implementation [50] can only work with helicity eigenstates. An extension of the Catani-Seymour formalism for randomly polarized partons has been recently presented in [63] and is characterized by the introduction of additional subtraction terms.

The basic idea of the random polarization method is to replace the polarization state with a linear combination of helicity eigenstates [64, 65]. For example, the polarization vector of a gluon is written as follows

$$\varepsilon^\mu(k, \phi) \equiv e^{i\phi} \varepsilon^\mu(k, +) + e^{-i\phi} \varepsilon^\mu(k, -), \quad (5.1)$$

where $\varepsilon^\mu(k, \pm)$ are the helicity eigenstates and $\phi \in [0, 2\pi]$ is a phase parameter. In this way one can replace a discrete sum over the helicities by an integration over the phase parameter ϕ according to the formula

$$\sum_\lambda |\mathcal{M}_\lambda|^2 = \frac{1}{2\pi} \int_0^{2\pi} d\phi |\mathcal{M}_\phi|^2. \quad (5.2)$$

In other words, this method extends the sampling phase space with additional degrees of freedom represented by the parameters ϕ 's, one for each randomly polarized particle. It should be clear that, in comparison with the approach of exact helicity summation, a higher number of points is required in order to reach the same integration accuracy. On the other hand, the computational complexity of the calculation is decreased in this way by a factor

³We note that evaluating the contributions from subtracted real part, **I** operator and **KP** operator in a single run instead of three separate steps, as proposed in [62], may improve the overall efficiency of the calculation especially in case of large cancellations between the various terms. We leave this optimization for future developments of the code.

$2^{n_2} 3^{n_3}$, where n_2 and n_3 denote the numbers of particles with 2 and 3 polarization states. Furthermore, since for every value of ϕ both helicities contribute, one does not expect large differences in the values of $|\mathcal{M}_\phi|^2$, and the resulting quasi-flat distribution in the Monte Carlo sampling should lead to an overall satisfactory convergence of the integration.

We provide *random polarization sampling* as a further option available for the Nagy-Soper scheme. This is an alternative to the existing *random helicity sampling* optimization, which uses stratified sampling over the different (incoherent) helicity assignments of partons [50]. The option for the spin sum treatment can be controlled by the user in the configuration file `dipoles.conf`. A detailed description of this files is reported in the Appendix.

Besides random polarization sampling, which is an important speedup in every calculation, we also provide *random sampling over color*, or *color Monte Carlo*, for the subtracted real radiation part. This functionality provides an important speedup for matrix elements with a large number of colored external states. We follow the general ideas from [4, 66], which are also an essential ingredient of HELAC-1LOOP. Consider a diagram with an arbitrary number of in- and/or out-going quarks, anti-quarks and gluons. We shall contract the gluon color index belonging to the adjoint representation with the generator matrix T_{ij}^a . Thus out-going quark and in-going anti-quark indices transform according to the $\mathbf{3}$ representation, out-going anti-quark and in-going quark indices according to the $\bar{\mathbf{3}}$ representation, whereas gluon indices according to the $\mathbf{3} \otimes \bar{\mathbf{3}}$ representation. Using the well-known identities

$$if^{abc} = \frac{1}{T_F} \text{Tr} \left(T^a T^b T^c - T^c T^b T^a \right) , \quad (5.3)$$

and

$$T_{ij}^a T_{kl}^a = T_F \left(\delta_{il} \delta_{kj} - \frac{1}{N_c} \delta_{ij} \delta_{kl} \right) , \quad (5.4)$$

one can reduce the contribution of any diagram to the form

$$\sum_{\sigma} \mathcal{A}(\sigma) \delta_{i_1 i_{\sigma(1)}} \cdots \delta_{i_n i_{\sigma(n)}} , \quad (5.5)$$

where the first index of every delta transforms according to the $\mathbf{3}$ representation and the second according to the $\bar{\mathbf{3}}$ representation, σ is a permutation, and $\mathcal{A}(\sigma)$ the amplitude corresponding to the given permutation. This representation is called the color flow representation, because the color “flows” from one index to the other within a link given by a delta function. The square of the amplitude summed over color is obtained by summing products of deltas over the indices. Internally, HELAC uses the color flow representation, but because summation over color mixes different color flows, the color Monte Carlo uses true color configurations. In fact, a single true color configuration is generated for every phase space point with a flat distribution. Subsequently, the color flows, which are compatible with this color configuration are determined. For this, it is sufficient to check which delta products in Eq.(5.5) do not vanish for the given assignment of the color indices. Finally, the amplitudes are evaluated for the color flows determined in this way. This approach speeds up the calculation by a large factor dependent on the process. Within a

subtraction scheme, it is important to have subtraction terms, which match the singularities of the amplitude for a given true color assignment. A given singular limit involves two partons in the collinear case, or three partons in the soft case. The colors of the remaining partons are simply copied from the original amplitude. During the determination of the color flows for the (color correlated) amplitude of the subtraction term, one then takes into account that a parton was obtained by merging two partons. For this, the color flows have to be generated according to Eq. (5.4) in order to correspond to a color correlator $\mathbf{T}_i \cdot \mathbf{T}_k$ insertion. Notice that, in case the splitting pair contains more than one gluon, one has to decide, which gluon is to be considered soft in the determination of the color flow (the missing index j from the color correlator). This is done by taking the gluon with the smaller energy as the soft one. One can show that such an approach reduces to the usual one (subtraction term amplitudes summed over color independently of the summation over color of the original amplitude) upon summation over all colors of the original amplitude. We have, of course, checked the pointwise convergence of our implementation for arbitrary configurations.

6 Numerical Study

6.1 Input parameters and phase space cuts

In order to test our implementation and compare it with that of the Catani-Seymour subtraction scheme, we have to choose some specific processes. Throughout this study we consider proton-proton collisions at the LHC with a center-of-mass energy of 8 TeV. We will concentrate on the following partonic subprocesses $gg \rightarrow t\bar{t}b\bar{b}g$, $gg \rightarrow t\bar{t}t\bar{t}g$, $gg \rightarrow b\bar{b}b\bar{b}g$, $gg \rightarrow t\bar{t}ggg$ that give dominant contributions to the subtracted real emissions at $\mathcal{O}(\alpha_s^5)$ for the corresponding processes $pp \rightarrow t\bar{t}b\bar{b} + X$, $pp \rightarrow t\bar{t}t\bar{t} + X$, $pp \rightarrow b\bar{b}b\bar{b} + X$ and $pp \rightarrow t\bar{t}jj + X$. These processes represent a high level of complexity and test almost all aspects of the software, as they involve both massive and massless states. Basic selection cuts are imposed on jets that are reconstructed via the IR-safe anti- k_T jet algorithm [67] with radius parameter $R = 1$. They are reconstructed out of all final-state partons that are lying in the pseudo-rapidity range accessible to the LHC detectors, *i.e.* within the range of $|\eta| < 5$. All jets are required to carry $p_T(j) > 50$ GeV and to be located in the rapidity-range of $|y(j)| < 2.5$. They are also made to be well separated in the rapidity-azimuthal angle plane with $\Delta R(jj) > 1$. Let us note that j corresponds to a light jet only, outgoing top and anti-top quarks are left on-shell, they do not comply to any cut selection. Let us also add, that in case of the $gg \rightarrow t\bar{t}ggg$ process jets are ordered according to their p_T and cuts are applied only on the two hardest jets. The mass of the top quark is set to $m_t = 173.5$ GeV [68], the bottom quark is considered to be massless. Results are presented for the NLO CT10 parton distribution functions [69] with five active flavors and the corresponding two-loop α_s . The renormalization and factorization scales are set to the scalar sum of the jet transverse masses, *i.e.*

$$H_T = \sum m_T(j), \quad (6.1)$$

where for the top quark $m_T(t) = \sqrt{m_t^2 + p_T^2(t)}$ and for light jets (also tagged bottom-jets) $m_T(j) = p_T(j)$. A factor of $1/4$ has been added for all but the $gg \rightarrow b\bar{b}b\bar{b}g$ process where $\mu_R = \mu_F = \mu_0 = H_T$ has been chosen instead. If not specified otherwise full summation over all color configurations is assumed together with random helicity sampling. The phase space integration is performed with the help of the Monte Carlo generator KALEU [70] including a multi-channel approach [71] for separate channels that are associated with the squared real emission matrix element along with each subtraction term [9]. The integration over the fractions of the momenta of the initial partons weighted by the parton distribution functions is performed with the help of PARNI [72].

6.2 Comparisons with the Catani-Seymour scheme

We now turn to a comparison of the Nagy-Soper subtraction scheme (NS), introduced in the previous sections, with the Catani-Seymour subtraction scheme (CS), widely used in the calculation of NLO QCD corrections. We start our comparison with the total number of subtraction terms that need to be evaluated in both schemes. They are presented in Table 1. The table also contains the number of Feynman diagrams corresponding to the subprocesses under scrutiny to underline their complexity. In each case, five times less terms are needed in the NS subtraction scheme compared to the CS scheme. The difference corresponds to the total number of possible spectators for a $2 \rightarrow 5$ process, which are relevant in the CS case, but not in the NS case.

Real emission cross sections together with their absolute and relative errors, the latter ones being expressed in %, are given in Table 2 and Table 3. Results are shown for the CS dipole subtraction, with ($\alpha_{max} = 0.01$) and without ($\alpha_{max} = 1$) restriction on the phase space of the subtraction [41, 73, 74], and the new NS scheme. All results are obtained for the same number of phase space points before cuts. We have used 64×10^6 points for both integrated subtraction terms, **I**- and **KP**, while for the subtracted real emission part $50 \times 20 \times 10^6$ phase-space points have been generated. For all cross sections the resulting relative errors are well below 1%, the largest one being five per mill, for details see Table 3. In addition, the actual maximal difference between two evaluations of a given cross section is twice the sum of the corresponding errors. However, on average, calculations coincide within the sum of two errors. The absolute errors given in Table 2 in the CS case with $\alpha_{max} = 0.01$ are noticeably higher than the corresponding ones for $\alpha_{max} = 1$, in fact by a factor of 2 – 4 depending on the process. However, this difference is reduced down to about 1.5 for the NS case vs the CS case with $\alpha_{max} = 1$. Thus, we do not observe dramatical differences between the NS and CS cases with $\alpha_{max} = 1$. These absolute errors are a consequence of the size of the errors of the three different contributions to the cross section. Since we have fixed the number of events for the single particle phase space integrated contributions (**I** and **KP** contributions) they might have an important effect on the final error. This is indeed the case for the CS scheme with $\alpha_{max} = 0.01$. As the **I** and **KP** contributions are not computationally intensive, a meaningful comparison of the schemes involves the subtracted real radiation contribution only. This comparison is performed below. Let us note, that we do not show any results for distributions, since such

comparisons have already been performed for some massive and massless cases in [23], and we are confident that the study of total cross sections is sufficient to draw conclusions on agreement and efficiency.

| PROCESS | NR. OF DIPOLES CATANI-SEYMOUR | NR. OF SUBTRACTIONS NAGY-SOPER | NR. OF FEYNMAN DIAGRAMS |
|------------------------------------|----------------------------------|-----------------------------------|----------------------------|
| $gg \rightarrow t\bar{t}b\bar{b}g$ | 55 | 11 | 341 |
| $gg \rightarrow t\bar{t}t\bar{t}g$ | 30 | 6 | 682 |
| $gg \rightarrow b\bar{b}b\bar{b}g$ | 90 | 18 | 682 |
| $gg \rightarrow t\bar{t}ggg$ | 75 | 15 | 1240 |

Table 1. Number of Catani-Seymour and Nagy-Soper subtraction terms for dominant partonic subprocesses contributing to the subtracted real emission contributions at $\mathcal{O}(\alpha_s^5)$ for the $pp \rightarrow t\bar{t}b\bar{b} + X$, $pp \rightarrow t\bar{t}t\bar{t} + X$, $pp \rightarrow b\bar{b}b\bar{b} + X$ and $pp \rightarrow t\bar{t}jj + X$ processes at the LHC. The number of Feynman diagrams corresponding to the subprocesses is given as well.

| PROCESS | $\sigma_{\text{RE}}^{\text{CS}(\alpha_{\text{max}}=0.01)}$ [pb] | $\sigma_{\text{RE}}^{\text{CS}(\alpha_{\text{max}}=1)}$ [pb] | $\sigma_{\text{RE}}^{\text{NS}}$ [pb] |
|------------------------------------|---|--|---------------------------------------|
| $gg \rightarrow t\bar{t}b\bar{b}g$ | $(28.43 \pm 0.13) \cdot 10^{-3}$ | $(28.39 \pm 0.04) \cdot 10^{-3}$ | $(28.59 \pm 0.06) \cdot 10^{-3}$ |
| $gg \rightarrow t\bar{t}t\bar{t}g$ | $(17.03 \pm 0.08) \cdot 10^{-5}$ | $(16.98 \pm 0.02) \cdot 10^{-5}$ | $(17.01 \pm 0.03) \cdot 10^{-5}$ |
| $gg \rightarrow b\bar{b}b\bar{b}g$ | $(65.71 \pm 0.30) \cdot 10^{-2}$ | $(66.24 \pm 0.16) \cdot 10^{-2}$ | $(66.06 \pm 0.22) \cdot 10^{-2}$ |
| $gg \rightarrow t\bar{t}ggg$ | $(87.91 \pm 0.17) \cdot 10^{-1}$ | $(87.96 \pm 0.07) \cdot 10^{-1}$ | $(88.16 \pm 0.08) \cdot 10^{-1}$ |

Table 2. Real emission cross sections for dominant partonic subprocesses contributing to the subtracted real emissions at $\mathcal{O}(\alpha_s^5)$ for the $pp \rightarrow t\bar{t}b\bar{b} + X$, $pp \rightarrow t\bar{t}t\bar{t} + X$, $pp \rightarrow b\bar{b}b\bar{b} + X$ and $pp \rightarrow t\bar{t}jj + X$ processes at the LHC. Results are shown for two different subtraction schemes, the Catani-Seymour (CS) dipole subtraction, with ($\alpha_{\text{max}} = 0.01$) and without ($\alpha_{\text{max}} = 1$) restriction on the phase space of the subtraction, and the new Nagy-Soper (NS) scheme, including the numerical error from the Monte Carlo integration.

We now turn our attention to the subtracted real emission part only. From the computation time point of view, this contribution is by far the dominant piece of the complete NLO calculation and the only one that requires a computer cluster. In Table 4 we present absolute errors of subtracted real emission cross sections again for both subtraction schemes and with or without a restriction on the phase space of the subtraction. Clearly, both schemes perform similarly and can be employed with confidence since final errors are of the same order. Let us note here however, that the number of accepted events (*i.e.* the efficiency of the phase space generator) for the three considered cases, CS with $\alpha_{\text{max}} = 1$,

| PROCESS | $\varepsilon_{\text{RE}}^{\text{CS}(\alpha_{\text{max}}=0.01)}$ [%] | $\varepsilon_{\text{RE}}^{\text{CS}(\alpha_{\text{max}}=1)}$ [%] | $\varepsilon_{\text{RE}}^{\text{NS}}$ [%] |
|------------------------------------|---|--|---|
| $gg \rightarrow t\bar{t}b\bar{b}g$ | 0.47 | 0.16 | 0.22 |
| $gg \rightarrow t\bar{t}t\bar{t}g$ | 0.51 | 0.11 | 0.19 |
| $gg \rightarrow b\bar{b}b\bar{b}g$ | 0.46 | 0.25 | 0.33 |
| $gg \rightarrow t\bar{t}ggg$ | 0.20 | 0.08 | 0.09 |

Table 3. Relative error in % on real emission cross sections for dominant partonic subprocesses contributing to the subtracted real emissions at $\mathcal{O}(\alpha_s^5)$ for the $pp \rightarrow t\bar{t}b\bar{b} + X$, $pp \rightarrow t\bar{t}t\bar{t} + X$, $pp \rightarrow b\bar{b}b\bar{b} + X$ and $pp \rightarrow t\bar{t}jj + X$ processes at the LHC. Results are shown for two different subtraction schemes, the Catani-Seymour (CS) dipole subtraction, with ($\alpha_{\text{max}} = 0.01$) and without ($\alpha_{\text{max}} = 1$) restriction on the phase space of the subtraction, and the new Nagy-Soper (NS) scheme.

| PROCESS | $\varepsilon_{\text{SR}}^{\text{CS}(\alpha_{\text{max}}=0.01)}$ [pb] | $\varepsilon_{\text{SR}}^{\text{CS}(\alpha_{\text{max}}=1)}$ [pb] | $\varepsilon_{\text{SR}}^{\text{NS}}$ [pb] |
|------------------------------------|--|---|--|
| $gg \rightarrow t\bar{t}b\bar{b}g$ | $4.405 \cdot 10^{-5}$ | $4.108 \cdot 10^{-5}$ | $5.424 \cdot 10^{-5}$ |
| $gg \rightarrow t\bar{t}t\bar{t}g$ | $1.356 \cdot 10^{-7}$ | $2.298 \cdot 10^{-8}$ | $2.377 \cdot 10^{-8}$ |
| $gg \rightarrow b\bar{b}b\bar{b}g$ | $1.271 \cdot 10^{-3}$ | $1.494 \cdot 10^{-3}$ | $2.027 \cdot 10^{-3}$ |
| $gg \rightarrow t\bar{t}ggg$ | $7.560 \cdot 10^{-3}$ | $2.290 \cdot 10^{-3}$ | $6.507 \cdot 10^{-3}$ |

Table 4. Absolute error for subtracted real emission cross sections for dominant partonic subprocesses contributing to the subtracted real emissions at $\mathcal{O}(\alpha_s^5)$ for the $pp \rightarrow t\bar{t}b\bar{b} + X$, $pp \rightarrow t\bar{t}t\bar{t} + X$, $pp \rightarrow b\bar{b}b\bar{b} + X$ and $pp \rightarrow t\bar{t}jj + X$ processes at the LHC. Results are shown for two different subtraction schemes, the Catani-Seymour (CS) dipole subtraction, with ($\alpha_{\text{max}} = 0.01$) and without ($\alpha_{\text{max}} = 1$) restriction on the phase space of the subtraction, and the new Nagy-Soper (NS) scheme.

CS with $\alpha_{\text{max}} = 0.01$ and NS, was slightly different. Just to give a general idea, for the $gg \rightarrow t\bar{t}b\bar{b}g$ subprocess the total number of the phase space points passing the cuts and contributing to the calculation of the real emission matrix element together with all the subtraction terms, was about 12×10^6 , 6×10^6 and 9×10^6 respectively, without including phase space points that have been evaluated in the optimization phase.

Finally, in Table 5, the time measured in milliseconds, needed to evaluate the real emission matrix element and the subtraction terms for one phase space point is given. All times correspond to $\alpha_{\text{max}} = 1$. When all subtraction terms are included, as it is the case for $\alpha_{\text{max}} = 1$, the CS subtraction scheme is slower by a factor of about three to four as compared to the cost of the pure real emission calculation. In case of the NS scheme, however, a slowdown of the order of 1.5 to 2 only is observed. We stress that if a restriction on the phase space of the subtraction is applied, corresponding to $\alpha_{\text{max}} \ll 1$, the cost of the subtracted real emission part is of the order of the cost of the real emission itself, *i.e* higher

| PROCESS | t^{CS} [msec] | t^{NS} [msec] | t^{RE} [msec] |
|------------------------------------|------------------------|------------------------|------------------------|
| $gg \rightarrow t\bar{t}b\bar{b}g$ | 24.8 | 13.2 | 6.5 |
| $gg \rightarrow t\bar{t}t\bar{t}g$ | 35.7 | 18.5 | 11.2 |
| $gg \rightarrow b\bar{b}b\bar{b}g$ | 26.6 | 16.2 | 10.1 |
| $gg \rightarrow t\bar{t}ggg$ | 214.8 | 108.2 | 48.7 |

Table 5. The CPU time needed to evaluate the real emission matrix element together with all the subtraction terms for one phase space point for two subtraction schemes, namely Catani-Seymour, t^{CS} (for $\alpha_{\text{max}} = 1$), and Nagy-Soper, t^{NS} . For comparison, we also give the CPU time for the pure real emission matrix element calculation, t^{RE} . All numbers have been obtained on an Intel 3.40 GHz processor with the Intel Fortran compiler using the option `-fast`.

only by about 10% – 15%. We have checked this for the CS case, where this restriction is implemented, assuming $\alpha_{\text{max}} = 0.01$. In that case, the total time for one phase space point has been estimated as an average from about 200 different phase space points, because for $\alpha_{\text{max}} \neq 1$ a different number of subtraction terms is evaluated for each phase space point.

Overall, both schemes, with their different momentum mappings and subtraction terms, have similar performance and give the same results for total real emission cross sections.

6.3 Random color and polarization sampling

In the last part on numerical results, we study the overall performance of Monte Carlo sampling over color and polarization. At the very beginning, real emission cross sections with absolute errors using random color sampling for two different subtraction schemes, the Catani-Seymour (CS) dipole subtraction, with ($\alpha_{\text{max}} = 0.01$) and without ($\alpha_{\text{max}} = 1$) restriction on the phase space of the subtraction, and the new Nagy-Soper (NS) scheme are given in Table 6. Relative errors expressed in % are shown in Table 7. We observe agreement with results presented in Table 2 where summation over all color flows has been performed. However, in the present case the absolute errors are 3 – 4 times higher, which is typical when Monte Carlo sampling is employed instead of full summation. Generally speaking, in order to obtain the same absolute errors 9 – 16 times more events would be required. In the case of $gg \rightarrow t\bar{t}b\bar{b}g$, $gg \rightarrow t\bar{t}t\bar{t}g$ and $gg \rightarrow b\bar{b}b\bar{b}g$ processes, which are the same from the color point of view, the total number of color flows is 120. Out of those only 98 give non-zero contributions and are evaluated for each phase space point for full summation over color. When Monte Carlo sampling is employed instead, the average number of color flows corresponding to a random color configuration is only 5. This gives a speed up of the order of 20 per phase space point, which is almost fully absorbed by the higher statistics that is required to obtain the same absolute error. Therefore, we conclude that for processes dominated by quarks random color sampling performs similarly to full color summation. On the other hand, in case of the $gg \rightarrow t\bar{t}ggg$ process, where the

| PROCESS | $\sigma_{\text{RE,COL}}^{\text{CS}(\alpha_{\text{max}}=0.01)}$ [pb] | $\sigma_{\text{RE,COL}}^{\text{CS}(\alpha_{\text{max}}=1)}$ [pb] | $\sigma_{\text{RE,COL}}^{\text{NS}}$ [pb] |
|------------------------------------|---|--|---|
| $gg \rightarrow t\bar{t}b\bar{b}g$ | $(28.91 \pm 0.32) \cdot 10^{-3}$ | $(28.35 \pm 0.14) \cdot 10^{-3}$ | $(28.77 \pm 0.14) \cdot 10^{-3}$ |
| $gg \rightarrow t\bar{t}t\bar{t}g$ | $(16.99 \pm 0.10) \cdot 10^{-5}$ | $(17.00 \pm 0.03) \cdot 10^{-5}$ | $(17.01 \pm 0.04) \cdot 10^{-5}$ |
| $gg \rightarrow b\bar{b}b\bar{b}g$ | $(67.01 \pm 0.64) \cdot 10^{-2}$ | $(65.71 \pm 0.50) \cdot 10^{-2}$ | $(67.00 \pm 0.66) \cdot 10^{-2}$ |
| $gg \rightarrow t\bar{t}g\bar{g}g$ | $(88.05 \pm 0.45) \cdot 10^{-1}$ | $(88.04 \pm 0.37) \cdot 10^{-1}$ | $(87.76 \pm 0.31) \cdot 10^{-1}$ |

Table 6. Real emission cross sections for dominant partonic subprocesses contributing to the subtracted real emissions at $\mathcal{O}(\alpha_s^5)$ for the $pp \rightarrow t\bar{t}b\bar{b} + X$, $pp \rightarrow t\bar{t}t\bar{t} + X$, $pp \rightarrow b\bar{b}b\bar{b} + X$ and $pp \rightarrow t\bar{t}jj + X$ processes at the LHC. Results are shown for random color sampling for two different subtraction schemes, the Catani-Seymour (CS) dipole subtraction, with ($\alpha_{\text{max}} = 0.01$) and without ($\alpha_{\text{max}} = 1$) restriction on the phase space of the subtraction, and the new Nagy-Soper (NS) scheme, including the numerical error from the Monte Carlo integration.

| PROCESS | $\varepsilon_{\text{RE,COL}}^{\text{CS}(\alpha_{\text{max}}=0.01)}$ [%] | $\varepsilon_{\text{RE,COL}}^{\text{CS}(\alpha_{\text{max}}=1)}$ [%] | $\varepsilon_{\text{RE,COL}}^{\text{NS}}$ [%] |
|------------------------------------|---|--|---|
| $gg \rightarrow t\bar{t}b\bar{b}g$ | 1.10 | 0.50 | 0.47 |
| $gg \rightarrow t\bar{t}t\bar{t}g$ | 0.60 | 0.18 | 0.23 |
| $gg \rightarrow b\bar{b}b\bar{b}g$ | 0.96 | 0.76 | 0.98 |
| $gg \rightarrow t\bar{t}g\bar{g}g$ | 0.52 | 0.42 | 0.35 |

Table 7. Relative error in % on real emission cross sections for dominant partonic subprocesses contributing to the subtracted real emissions at $\mathcal{O}(\alpha_s^5)$ for the $pp \rightarrow t\bar{t}b\bar{b} + X$, $pp \rightarrow t\bar{t}t\bar{t} + X$, $pp \rightarrow b\bar{b}b\bar{b} + X$ and $pp \rightarrow t\bar{t}jj + X$ processes at the LHC. Results are shown for random color sampling for two different subtraction schemes, the Catani-Seymour (CS) dipole subtraction, with ($\alpha_{\text{max}} = 0.01$) and without ($\alpha_{\text{max}} = 1$) restriction on the phase space of the subtraction, and the new Nagy-Soper (NS) scheme.

number of gluons is much higher, the number of all, non-zero and average color flows per phase space point is 720, 326 and 6 respectively. Here the speed up per phase space point is of the order of 50 and therefore still clearly visible even if a higher number of events is generated. Therefore, we draw the conclusion that random color sampling is a powerful approach mostly for processes where the number of gluons is higher and exceeds the number of quarks.

Finally, in Table 8 real emission cross sections for random polarization sampling for the new Nagy-Soper (NS) subtraction scheme, including numerical errors from the Monte Carlo integration are shown. Also given there are their relative errors in %. When comparing the numbers presented with results from Table 2 and Table 3 (last column in both cases) where we make use of random helicity sampling, not only a perfect agreement can be noticed but also the same absolute and relative errors can be found. In addition, the CPU time that is

| PROCESS | $\sigma_{\text{RE,POL}}^{\text{NS}}$ [pb] | $\epsilon_{\text{RE,POL}}^{\text{NS}}$ [%] |
|------------------------------------|---|--|
| $gg \rightarrow t\bar{t}b\bar{b}g$ | $(28.50 \pm 0.06) \cdot 10^{-3}$ | 0.21 |
| $gg \rightarrow t\bar{t}t\bar{t}g$ | $(17.01 \pm 0.03) \cdot 10^{-5}$ | 0.19 |
| $gg \rightarrow b\bar{b}b\bar{b}g$ | $(66.23 \pm 0.20) \cdot 10^{-2}$ | 0.30 |
| $gg \rightarrow t\bar{t}ggg$ | $(88.16 \pm 0.07) \cdot 10^{-1}$ | 0.08 |

Table 8. Real emission cross sections for dominant partonic subprocesses contributing to the subtracted real emissions at $\mathcal{O}(\alpha_s^5)$ for the $pp \rightarrow t\bar{t}b\bar{b} + X$, $pp \rightarrow t\bar{t}t\bar{t} + X$, $pp \rightarrow b\bar{b}b\bar{b} + X$ and $pp \rightarrow t\bar{t}jj + X$ processes at the LHC. Results are shown for random polarization sampling for the new Nagy-Soper (NS) subtraction scheme, including the numerical error from the Monte Carlo integration. Also given are relative errors in %.

needed for the evaluation of one phase space point is similar in both cases, which clearly tells us that for the processes under consideration both methods behave similarly and can be used interchangeably. Moreover, these two different approaches can be utilized to test and compare results.

7 Conclusions and Outlook

In this paper, we have presented the details of a complete implementation of the Nagy-Soper subtraction scheme. The most important aspect was the integration of the subtraction terms over the one-particle unresolved phase space. We have achieved this by using a semi-numerical approach, where the azimuthal angle is integrated analytically, while the remaining angle and energy are integrated numerically after suitable subtraction. We have implemented our approach within the HELAC-DIPOLES framework making use of the existing structure designed for the Catani-Seymour dipole subtraction scheme. Thanks to the structure of the splitting functions in the Nagy-Soper scheme, which are given in terms of actual spinors and polarization vectors, we were able to provide random polarization Monte Carlo summation over spins instead of full summation or random helicity sampling, which is used in the Catani-Seymour case. Additionally, we have implemented Monte Carlo summation over color by generating random true color assignments and translating them into the color flow language. This last optimization will be most useful in large calculations for many parton final states.

Having two different subtraction schemes available within the same software allowed us to make efficiency comparisons. There are two aspects, when comparing Catani-Seymour and Nagy-Soper subtraction. The first aspect is the evaluation time needed to obtain the contribution of the real radiation and the subtraction terms for a given phase space point. By design, the Nagy-Soper scheme has less kinematical mappings and should therefore be faster. This is indeed what we could observe. In our applications with a moderate number of final state partons (five), the differences are less than a factor of two in favor

of Nagy-Soper subtraction as long as there is no restriction on the dipole phase space in the Catani-Seymour scheme. With a low cutoff in the latter scheme, both approaches are very similar as far as time is concerned. The second aspect is the convergence rate of the integration. We used the same phase space generator, KALEU in our comparisons and assumed the same number of generated points. We observed that the absolute error of the most costly (in terms of computational time) contribution was slightly worse for Nagy-Soper than for Catani-Seymour without phase space restriction. In the end, we are forced to conclude that both schemes are similar in efficiency. We do not consider differences below a factor of two in error or time (which are moreover process dependent) a reason to prefer either scheme.

There are two advantages of our implementation. The first is that we can now perform better tests in applications by computing real radiation in two different schemes. The second is that the integrated subtraction terms can be used to match the fixed order calculation onto the Nagy-Soper parton shower. This will be the subject of our future work. Another direction of research is the implementation of the phase space cutoffs on the subtraction terms in the Nagy-Soper scheme. We would also like to investigate, whether having such a restriction and combining the evaluation of subtracted real radiation and integrated subtraction terms on a point-by-point basis could improve the convergence of the calculation.

Finally, let us stress that the software developed in the course of this work is publicly available⁴.

Acknowledgments

We acknowledge useful discussions with M.Krämer and Z.Nagy.

This research was supported by the German Research Foundation (DFG) via the Sonderforschungsbereich/Transregio SFB/TR-9 “*Computational Particle Physics*”. M.C. was also supported by the Heisenberg programme of the DFG. M.W. acknowledges support by the DFG under Grant No. WO 1900/1-1 (“*Signals and Backgrounds Beyond Leading Order. Phenomenological studies for the LHC*”).

A Configuration of HELAC-DIPOLES

In this Appendix we provide an updated description of the `dipoles.conf` file, which is the configuration file where the user can set specific parameters for the calculation of the subtracted real part. For a more complete description of the program setup we refer to [33].

- `dipoletype`: type of the subtraction scheme: 0 - Catani-Seymour, 1 - Nagy-Soper.
- `onlyreal`: if set to true, only real emission, without subtraction terms, is calculated. The cuts are specified in `cuts.h`. The result must coincide with the one of the original

⁴<http://helac-phegas.web.cern.ch/helac-phegas/helac-dipoles.html>.

HELAC-PHEGAS with the same input parameters. This option is included for testing purposes.

- **onlylast**: if set to true, only those dipoles will be included, which contain the last particle (for correctness it must be a parton). This is useful for some processes, where it is clear that only the last particle can be soft/collinear, and the bookkeeping remains simple to obtain the full result at NLO.
- **onlydiv**: if set to true, only divergent dipoles will be included. Non-divergent dipoles correspond to a pair of massive quarks in the final state. They are only useful to get rid of large Sudakov logarithms, but are not essential for the finiteness of the real radiation contribution. For the Nagy-Soper scheme, non-divergent subtractions are not available in the present version.
- **hybrid**: if set to true, non-parton polarizations will be summed over by a continuous Monte Carlo integration over a phase parameter.
- **signmode**: defines how positive and negative contributions are to be treated: 0 - the result is left unchanged, both positive and negative results are included, 1 - only positive numbers, a negative result is set to zero, 2 - only negative numbers, but with the changed sign, positive results are set to zero.
- **sumtype**: in the first phase (preferably during the phase-space optimization), the summation over helicities of the partons can be performed in three different ways: 0 - exact fast summation (independently for real radiation and dipoles), 1 - exact slow summation (for a given helicity configuration both real radiation and the dipole sum will be calculated), 2 - Monte Carlo summation over all non-vanishing helicity configurations with multichannel optimization. In practice, option 2 is recommended. For the Nagy-Soper scheme an additional option is available: 3 - random polarization sampling. In this case, sampling is used throughout the calculation, *i.e.* also during the phase space optimization.
- **nsumpol**: number of accepted points to be summed over helicity with the method specified by sumtype. The counting starts after phase space optimization is finished.
- **noptpol**: number of accepted points to be used for helicity sampling optimization. During helicity sampling optimization, slow summation over helicity configurations (in the sense defined in the description of sumtype) is performed. It is therefore recommended to keep this number relatively small (of the order of a few hundred to a thousand).
- **nuptpol**: number of accepted points after which an update of the helicity sampling weights is performed. This number should be rather large for best results (at least an order of magnitude larger than noptpol).

- **alphaMinCut**: lowest value of α_{min} , below which a point will be rejected altogether, because of the risk of numerical instabilities. For the exact definition of α_{min} , see *e.g.* [50].
- **alphaMaxII**, **alphaMaxIF**, **alphaMaxFI**, **alphaMaxFF**, **kappa**: parameters for a restriction on the phase space of the subtraction in the Catani-Seymour scheme (see [50]). For the Nagy-Soper scheme, no phase-space restriction is available in the present version.
- **colorsampling**: if set to true, Monte Carlo color sampling is performed.
- **jet algorithm**: type of jet algorithm: 1 - k_T , -1 - anti- k_T , 0 - Cambridge/Aachen, see *e.g.* [75].
- **number of b -jets**: number of tagged bottom-jets in the final state.
- **max. pseudorapidity of clustered partons**, **jet resolution parameter**: η_{max} and R , parameters that shape the jet algorithm.
- **jetveto**: if set to true, additional jet radiation is vetoed.
- **ptveto**: maximum allowed p_T for the extra jet, in case a jet veto is active.

References

- [1] C. F. Berger, Z. Bern, L. J. Dixon, F. Febres Cordero, D. Forde, T. Gleisberg, H. Ita and D. A. Kosower *et al.*, “Precise Predictions for $W + 3$ Jet Production at Hadron Colliders,” Phys. Rev. Lett. **102** (2009) 222001 [arXiv:0902.2760 [hep-ph]].
- [2] A. Bredenstein, A. Denner, S. Dittmaier and S. Pozzorini, “NLO QCD corrections to $pp \rightarrow t$ anti- t b anti- b + X at the LHC,” Phys. Rev. Lett. **103** (2009) 012002 [arXiv:0905.0110 [hep-ph]].
- [3] R. K. Ellis, K. Melnikov and G. Zanderighi, “W+3 jet production at the Tevatron,” Phys. Rev. D **80** (2009) 094002 [arXiv:0906.1445 [hep-ph]].
- [4] G. Bevilacqua, M. Czakon, C. G. Papadopoulos, R. Pittau and M. Worek, “Assault on the NLO Wishlist: $pp \rightarrow t\bar{t}b\bar{b}$,” JHEP **0909** (2009) 109 [arXiv:0907.4723 [hep-ph]].
- [5] A. Bredenstein, A. Denner, S. Dittmaier and S. Pozzorini, “NLO QCD Corrections to Top Anti-Top Bottom Anti-Bottom Production at the LHC: 2. full hadronic results,” JHEP **1003** (2010) 021 [arXiv:1001.4006 [hep-ph]].
- [6] G. Bevilacqua, M. Czakon, C. G. Papadopoulos and M. Worek, “Dominant QCD Backgrounds in Higgs Boson Analyses at the LHC: A Study of $pp \rightarrow t$ anti- t + 2 jets at Next-To-Leading Order,” Phys. Rev. Lett. **104** (2010) 162002 [arXiv:1002.4009 [hep-ph]].
- [7] C. F. Berger, Z. Bern, L. J. Dixon, F. Febres Cordero, D. Forde, T. Gleisberg, H. Ita and D. A. Kosower *et al.*, “Precise Predictions for $W + 4$ Jet Production at the Large Hadron Collider,” Phys. Rev. Lett. **106** (2011) 092001 [arXiv:1009.2338 [hep-ph]].
- [8] A. Denner, S. Dittmaier, S. Kallweit and S. Pozzorini, “NLO QCD corrections to WWbb production at hadron colliders,” Phys. Rev. Lett. **106** (2011) 052001 [arXiv:1012.3975 [hep-ph]].

- [9] G. Bevilacqua, M. Czakon, A. van Hameren, C. G. Papadopoulos and M. Worek, “Complete off-shell effects in top quark pair hadroproduction with leptonic decay at next-to-leading order,” JHEP **1102** (2011) 083 [arXiv:1012.4230 [hep-ph]].
- [10] T. Melia, K. Melnikov, R. Rontsch and G. Zanderighi, “NLO QCD corrections for W^+W^- pair production in association with two jets at hadron colliders,” Phys. Rev. D **83** (2011) 114043 [arXiv:1104.2327 [hep-ph]].
- [11] N. Greiner, A. Guffanti, T. Reiter and J. Reuter, “NLO QCD corrections to the production of two bottom anti-bottom pairs at the LHC,” Phys. Rev. Lett. **107** (2011) 102002 [arXiv:1105.3624 [hep-ph]].
- [12] F. Campanario, C. Englert, M. Rauch and D. Zeppenfeld, “Precise predictions for $W\gamma\gamma$ +jet production at hadron colliders,” Phys. Lett. B **704** (2011) 515 [arXiv:1106.4009 [hep-ph]].
- [13] G. Bevilacqua, M. Czakon, C. G. Papadopoulos and M. Worek, “Hadronic top-quark pair production in association with two jets at Next-to-Leading Order QCD,” Phys. Rev. D **84** (2011) 114017 [arXiv:1108.2851 [hep-ph]].
- [14] S. Becker, D. Goetz, C. Reuschle, C. Schwan and S. Weinzierl, “NLO results for five, six and seven jets in electron-positron annihilation,” Phys. Rev. Lett. **108** (2012) 032005 [arXiv:1111.1733 [hep-ph]].
- [15] Z. Bern, G. Diana, L. J. Dixon, F. Febres Cordero, S. Hoeche, D. A. Kosower, H. Ita and D. Maitre *et al.*, “Four-Jet Production at the Large Hadron Collider at Next-to-Leading Order in QCD,” Phys. Rev. Lett. **109** (2012) 042001 [arXiv:1112.3940 [hep-ph]].
- [16] M. Worek, “On the next-to-leading order QCD K-factor for top anti-top bottom anti-bottom production at the TeVatron,” JHEP **1202** (2012) 043 [arXiv:1112.4325 [hep-ph]].
- [17] N. Greiner, G. Heinrich, P. Mastrolia, G. Ossola, T. Reiter and F. Tramontano, “NLO QCD corrections to the production of W^+W^- plus two jets at the LHC,” Phys. Lett. B **713** (2012) 277 [arXiv:1202.6004 [hep-ph]].
- [18] G. Bevilacqua and M. Worek, “Constraining BSM Physics at the LHC: Four top final states with NLO accuracy in perturbative QCD,” JHEP **1207** (2012) 111 [arXiv:1206.3064 [hep-ph]].
- [19] A. Denner, S. Dittmaier, S. Kallweit and S. Pozzorini, “NLO QCD corrections to off-shell top-antitop production with leptonic decays at hadron colliders,” JHEP **1210** (2012) 110 [arXiv:1207.5018 [hep-ph]].
- [20] S. Badger, B. Biedermann, P. Uwer and V. Yundin, “NLO QCD corrections to multi-jet production at the LHC with a centre-of-mass energy of $\sqrt{s} = 8$ TeV,” Phys. Lett. B **718** (2013) 965 [arXiv:1209.0098 [hep-ph]].
- [21] A. Denner, L. Hosekova and S. Kallweit, “NLO QCD corrections to W^+W^+ jj production in vector-boson fusion at the LHC,” Phys. Rev. D **86** (2012) 114014 [arXiv:1209.2389 [hep-ph]].
- [22] Z. Bern, L. J. Dixon, F. Febres Cordero, S. Hoeche, H. Ita, D. A. Kosower, D. Maitre and K. J. Ozeren, “Next-to-Leading Order $W + 5$ -Jet Production at the LHC,” Phys. Rev. D **88**, (2013) 014025 [arXiv:1304.1253 [hep-ph]].
- [23] G. Bevilacqua, M. Czakon, M. Krämer, M. Kubocz and M. Worek, “Quantifying quark mass effects at the LHC: A study of $pp \rightarrow b\bar{b}b\bar{b} + X$ at next-to-leading order,” JHEP **1307** (2013) 095 [arXiv:1304.6860 [hep-ph]].

- [24] F. Campanario and M. Kubocz, “Higgs boson production in association with three jets via gluon fusion at the LHC: Gluonic contributions,” *Phys. Rev. D* **88** (2013) 054021 [arXiv:1306.1830 [hep-ph]].
- [25] G. Cullen, H. van Deurzen, N. Greiner, G. Luisoni, P. Mastrolia, E. Mirabella, G. Ossola and T. Peraro *et al.*, “NLO QCD corrections to Higgs boson production plus three jets in gluon fusion,” *Phys. Rev. Lett.* **111** (2013) 131801 [arXiv:1307.4737 [hep-ph]].
- [26] H. van Deurzen, G. Luisoni, P. Mastrolia, E. Mirabella, G. Ossola and T. Peraro, “NLO QCD corrections to Higgs boson production in association with a top quark pair and a jet,” *Phys. Rev. Lett.* **111** (2013) 171801 [arXiv:1307.8437 [hep-ph]].
- [27] T. Gehrmann, N. Greiner and G. Heinrich, “Precise QCD predictions for the production of a photon pair in association with two jets,” arXiv:1308.3660 [hep-ph].
- [28] Z. Bern, L. J. Dixon, D. C. Dunbar and D. A. Kosower, “One loop n point gauge theory amplitudes, unitarity and collinear limits,” *Nucl. Phys. B* **425** (1994) 217 [hep-ph/9403226].
- [29] R. Britto, F. Cachazo and B. Feng, “Generalized unitarity and one-loop amplitudes in N=4 super-Yang-Mills,” *Nucl. Phys. B* **725** (2005) 275 [hep-th/0412103].
- [30] G. Ossola, C. G. Papadopoulos and R. Pittau, “Reducing full one-loop amplitudes to scalar integrals at the integrand level,” *Nucl. Phys. B* **763** (2007) 147 [hep-ph/0609007].
- [31] W. T. Giele, Z. Kunszt and K. Melnikov, “Full one-loop amplitudes from tree amplitudes,” *JHEP* **0804** (2008) 049 [arXiv:0801.2237 [hep-ph]].
- [32] A. van Hameren, C. G. Papadopoulos and R. Pittau, “Automated one-loop calculations: A Proof of concept,” *JHEP* **0909** (2009) 106 [arXiv:0903.4665 [hep-ph]].
- [33] G. Bevilacqua, M. Czakon, M. V. Garzelli, A. van Hameren, A. Kardos, C. G. Papadopoulos, R. Pittau and M. Worek, “HELAC-NLO,” *Comput. Phys. Commun.* **184** (2013) 986 [arXiv:1110.1499 [hep-ph]].
- [34] G. Cullen, N. Greiner, G. Heinrich, G. Luisoni, P. Mastrolia, G. Ossola, T. Reiter and F. Tramontano, “Automated One-Loop Calculations with GoSam,” *Eur. Phys. J. C* **72** (2012) 1889 [arXiv:1111.2034 [hep-ph]].
- [35] F. Cascioli, P. Maierhofer and S. Pozzorini, “Scattering Amplitudes with Open Loops,” *Phys. Rev. Lett.* **108** (2012) 111601 [arXiv:1111.5206 [hep-ph]].
- [36] S. Actis, A. Denner, L. Hofer, A. Scharf and S. Uccirati, “Recursive generation of one-loop amplitudes in the Standard Model,” *JHEP* **1304** (2013) 037 [arXiv:1211.6316 [hep-ph]].
- [37] T. Binoth, J. P. Guillet, G. Heinrich, E. Pilon and C. Schubert, “An Algebraic/numerical formalism for one-loop multi-leg amplitudes,” *JHEP* **0510** (2005) 015 [hep-ph/0504267].
- [38] A. Denner and S. Dittmaier, “Reduction schemes for one-loop tensor integrals,” *Nucl. Phys. B* **734** (2006) 62 [hep-ph/0509141].
- [39] K. Arnold, M. Bahr, G. Bozzi, F. Campanario, C. Englert, T. Figy, N. Greiner and C. Hackstein *et al.*, “VBFNLO: A Parton level Monte Carlo for processes with electroweak bosons,” *Comput. Phys. Commun.* **180** (2009) 1661 [arXiv:0811.4559 [hep-ph]].
- [40] G. Cullen, J. P. Guillet, G. Heinrich, T. Kleinschmidt, E. Pilon, T. Reiter and M. Rodgers, “Golem95C: A library for one-loop integrals with complex masses,” *Comput. Phys. Commun.* **182** (2011) 2276 [arXiv:1101.5595 [hep-ph]].
- [41] S. Frixione, Z. Kunszt and A. Signer, “Three jet cross-sections to next-to-leading order,”

- Nucl. Phys. B **467** (1996) 399 [hep-ph/9512328].
- [42] S. Catani and M. H. Seymour, “A General algorithm for calculating jet cross-sections in NLO QCD,” Nucl. Phys. B **485** (1997) 291 [Erratum-ibid. B **510** (1998) 503] [hep-ph/9605323].
- [43] Z. Nagy and D. E. Soper, “Parton showers with quantum interference,” JHEP **0709** (2007) 114 [arXiv:0706.0017 [hep-ph]].
- [44] Z. Nagy and D. E. Soper, “Parton showers with quantum interference: Leading color, spin averaged,” JHEP **0803** (2008) 030 [arXiv:0801.1917 [hep-ph]].
- [45] Z. Nagy and D. E. Soper, “Parton showers with quantum interference: Leading color, with spin,” JHEP **0807** (2008) 025 [arXiv:0805.0216 [hep-ph]].
- [46] C. H. Chung, M. Kramer and T. Robens, “An alternative subtraction scheme for next-to-leading order QCD calculations,” JHEP **1106** (2011) 144 [arXiv:1012.4948 [hep-ph]].
- [47] C. -H. Chung and T. Robens, “Nagy-Soper subtraction scheme for multiparton final states,” Phys. Rev. D **87** (2013) 074032 [arXiv:1209.1569 [hep-ph]].
- [48] T. Robens, “Nagy-Soper subtraction: a review,” Mod. Phys. Lett. A, Vol. 28, No. **23** (2013) 1330020 [arXiv:1306.1946 [hep-ph]].
- [49] M. Czakon, “A novel subtraction scheme for double-real radiation at NNLO,” Phys. Lett. B **693** (2010) 259 [arXiv:1005.0274 [hep-ph]].
- [50] M. Czakon, C. G. Papadopoulos and M. Worek, “Polarizing the Dipoles,” JHEP **0908** (2009) 085 [arXiv:0905.0883 [hep-ph]].
- [51] S. Catani, S. Dittmaier, M. H. Seymour and Z. Trocsanyi, “The Dipole formalism for next-to-leading order QCD calculations with massive partons,” Nucl. Phys. B **627** (2002) 189 [hep-ph/0201036].
- [52] G. Altarelli and G. Parisi, “Asymptotic Freedom in Parton Language,” Nucl. Phys. B **126** (1977) 298.
- [53] A. Kanaki and C. G. Papadopoulos, “HELAC: A Package to compute electroweak helicity amplitudes,” Comput. Phys. Commun. **132** (2000) 306 [hep-ph/0002082].
- [54] C. G. Papadopoulos, “PHEGAS: A Phase space generator for automatic cross-section computation,” Comput. Phys. Commun. **137** (2001) 247 [hep-ph/0007335].
- [55] A. Kanaki and C. G. Papadopoulos, “HELAC-PHEGAS: Automatic computation of helicity amplitudes and cross-sections,” hep-ph/0012004.
- [56] A. Cafarella, C. G. Papadopoulos and M. Worek, “Helac-Phegas: A Generator for all parton level processes,” Comput. Phys. Commun. **180** (2009) 1941 [arXiv:0710.2427 [hep-ph]].
- [57] P. Mastrolia, G. Ossola, C. G. Papadopoulos and R. Pittau, “Optimizing the Reduction of One-Loop Amplitudes,” JHEP **0806** (2008) 030 [arXiv:0803.3964 [hep-ph]].
- [58] G. Ossola, C. G. Papadopoulos and R. Pittau, “CutTools: A Program implementing the OPP reduction method to compute one-loop amplitudes,” JHEP **0803** (2008) 042 [arXiv:0711.3596 [hep-ph]].
- [59] G. Ossola, C. G. Papadopoulos and R. Pittau, “On the Rational Terms of the one-loop amplitudes,” JHEP **0805** (2008) 004 [arXiv:0802.1876 [hep-ph]].
- [60] P. Draggiotis, M. V. Garzelli, C. G. Papadopoulos and R. Pittau, “Feynman Rules for the Rational Part of the QCD 1-loop amplitudes,” JHEP **0904** (2009) 072 [arXiv:0903.0356

- [hep-ph]].
- [61] A. van Hameren, “OneLOop: For the evaluation of one-loop scalar functions,” *Comput. Phys. Commun.* **182** (2011) 2427 [arXiv:1007.4716 [hep-ph]].
 - [62] Z. Nagy and Z. Trocsanyi, “Calculation of QCD jet cross-sections at next-to-leading order,” *Nucl. Phys. B* **486** (1997) 189 [hep-ph/9610498].
 - [63] D. Goetz, C. Schwan and S. Weinzierl, “Random Polarizations of the Dipoles,” *Phys. Rev. D* **85** (2012) 116011 [arXiv:1205.4109 [hep-ph]].
 - [64] P. Draggotis, R. H. P. Kleiss and C. G. Papadopoulos, *Phys. Lett. B* **439** (1998) 157 [hep-ph/9807207].
 - [65] P. D. Draggotis, R. H. P. Kleiss and C. G. Papadopoulos, *Eur. Phys. J. C* **24** (2002) 447 [hep-ph/0202201].
 - [66] C. G. Papadopoulos and M. Worek, “Multi-parton cross sections at hadron colliders,” *Eur. Phys. J. C* **50** (2007) 843 [hep-ph/0512150].
 - [67] M. Cacciari, G. P. Salam and G. Soyez, “The Anti-k(t) jet clustering algorithm,” *JHEP* **0804** (2008) 063 [arXiv:0802.1189 [hep-ph]].
 - [68] J. Beringer *et al.* [Particle Data Group Collaboration], “Review of Particle Physics (RPP),” *Phys. Rev. D* **86** (2012) 010001.
 - [69] H. -L. Lai, M. Guzzi, J. Huston, Z. Li, P. M. Nadolsky, J. Pumplin and C. -P. Yuan, “New parton distributions for collider physics,” *Phys. Rev. D* **82** (2010) 074024 [arXiv:1007.2241 [hep-ph]].
 - [70] A. van Hameren, “Kaleu: A General-Purpose Parton-Level Phase Space Generator,” arXiv:1003.4953 [hep-ph].
 - [71] R. Kleiss and R. Pittau, “Weight optimization in multichannel Monte Carlo,” *Comput. Phys. Commun.* **83** (1994) 141 [hep-ph/9405257].
 - [72] A. van Hameren, “PARNI for importance sampling and density estimation,” *Acta Phys. Polon. B* **40** (2009) 259 [arXiv:0710.2448 [hep-ph]].
 - [73] Z. Nagy and Z. Trocsanyi, “Next-to-leading order calculation of four jet observables in electron positron annihilation,” *Phys. Rev. D* **59** (1999) 014020 [Erratum-ibid. *D* **62** (2000) 099902] [hep-ph/9806317].
 - [74] Z. Nagy, “Next-to-leading order calculation of three jet observables in hadron hadron collision,” *Phys. Rev. D* **68** (2003) 094002 [hep-ph/0307268].
 - [75] G. P. Salam, “Towards Jetography,” *Eur. Phys. J. C* **67** (2010) 637 [arXiv:0906.1833 [hep-ph]].